CALIFORNIA STATE UNIVERSITY, NORTHRIDGE

Late Pleistocene Slip Rate for the Western Pinto Mountain Fault, Morongo Valley, Southern California

A Thesis submitted in partial fulfillment of the requirements
For the degree of Master of Science in Geology

By

Katherine Gabriel

August, 2017

The thesis of Katherine Gabriel is approved:

_____	_____
Dr. Richard Heermance,	Date
_____	_____
Dr. Julian Lozos	Date
_____	_____
Dr. Doug Yule, Chair	Date

California State University, Northridge

ACKNOWLEDGMENTS

This project was made possible with funding from the Southern California Earthquake Center, Geological Society of America and the South Coast Geological Society. I would like to thank Marilyn Hanna for her generous financial support and unwavering enthusiasm for the geosciences at CSUN. I am very grateful for my committee members, Dr. Richard Heermance, Dr. Julian Lozos, and Dr. Doug Yule (committee chair) for their help throughout the research and writing process. Particular thanks to Dr. Doug Yule and Dr. Richard Heermance for their patience and dedication in the field and lab. Thank you to Katherine Kendrick (USGS) for contributing her time and expertise to this project. I would also like to than William Cochran (Virginia Tech) for kindly and generously providing early access to the Lidar data collected in my field area and for donating his time and equipment to collection of photos for Structure from Motion survey for this project. I am so grateful to my family and friends for their unconditional support throughout this project.

TABLE OF CONTENTS

Signature Page……... ii

ACKNOWLEDGEMENTS……...iii

LIST OF FIGURES……... vi

ABSTRACT……...vii

INTRODUCTION…… 1

GEOLOGIC BACKGROUND……..4

San Andreas Fault System……... 4

Pinto Mountain Fault……. 5

Regional Controls on Fan Formation…….8

METHODS…… 9

Geologic and Digital Elevation Model Data Collection…… 9

Fault Offset……10

In Situ Terrestrial Cosmogenic Exposure Dating…….. 11

RESULTS……..... 14

Geology……..14

Fault Outcrops and Pleistocene Offset……...15

Holocene Fault Offset…… 17

Geochronology……...18

Slip Rates……... 19

DISCUSSION …….... 21

Geochronology Uncertainties…… 21

Regional Correlation of Surfaces……...22

Fault Scarps……24

Offset Uncertainties……... 25

Tectonic Implications…..……..26

Slip Rate Implications……28

CONCLUSIONS……30

REFERENCES CITED……..32

APPENDIX A: FIGURES……37

APPENDIX B: TABLES……56

LIST OF FIGURES

Figure 1: Simplified regional fault map…… 37

Figure 2: Lidar and structure from motion data…….38

Figure 3: Geologic map of the study area……..39

Figure 4: Process of surface deflation……40

Figure 5: Photos of geologic units…… 41

Figure 6: Boulders from Qa and Qoa…….42

Figure 7: Outcrop of the main splay of the Pinto Mountain fault……..43

Figure 8: Outcrop of north splay of the Pinto Mountain fault along fault plane…....44

Figure 9: Outcrop of northern splay of the Pinto Mountain fault……...45

Figure 10: Lidar of the modern incised channel……....….46

Figure 11: North splay scarp…….....……..47

Figure 12: 3D structure from motion model…….....48

Figure13: Lidar image showing stream sinuosity…….…....49

Figure 14: Photos of boulders sampled for cosmogenic ^{10}Be……....….....50

Figure 15: Sample age plot…….....……..51

Figure 16: Histogram results of 10,000 Monte Carlo analyses of slip rate…...….....52

Figure 17 Schematic topographic profile of terrace levels…….…...…..53

Figure 18: Restoration of offset across the PMF system…….....54

Figure 19: Restoration of offset modern channel incised into Qoa…….....55

ABSTRACT

Late Pleistocene Slip Rate for the Western Pinto Mountain Fault, Morongo Valley, Southern California

By

Katherine Gabriel

Master of Science in Geology

The San Gorgonio Pass (SGP) region of the San Andreas fault (SAF) system in southern California is complicated by overlapping, active strands and its intersection with prominent, secondary structures such as the Pinto Mountain fault (PMF). Recent work in this area proposes that strain may be transferred from the Mission Creek strand of the SAF to the Eastern California Shear Zone (ECSZ), at least partly via the PMF. Like the better known Garlock fault, the PMF is a major east-west trending left-lateral transverse fault that intersects the Mission Creek strand of the SAF in the eastern SGP area. Geodetic and geologic slip rates reported for the PMF vary from 1 to 12.5 mm/yr and are poorly constrained because of a lack of geologic data.

This report describes a geologic slip rate from faulted alluvium in Big Morongo Canyon in Morongo Valley, California. A best-constrained strath contact between late Pleistocene alluvium (Qoa) and underlying bedrock (ggm) is offset in a left-lateral sense a total of 228 – 303 m. I obtained cosmogenic ^{10}Be exposure ages of six monzo-granite boulders on the surface of Qoa. Assuming zero-erosion rate, boulder ages range from ~63

ka to ~88 ka. I believe that surface deflation and erosion has occurred, and therefore choose a weighted average of 86.9 +/- 4.5 ka as the preferred age for the surface of Qoa. I calculate a preferred slip rate of 3.0 +0.6/-0.4 mm/yr for western PMF system for the last ~87 ka.

A fault scarp on one of the secondary splays in latest Pleistocene to Holocene alluvium (Qa) indicates that the western PMF has been active during the last <~15 ka. Results presented here support a model whereby the PMF represents a direct connection between the Mission Creek strand of the SAF to the ECSZ and contributes to a decrease in the slip rate on the SAF system through the SGP region.

INTRODUCTION

Through the San Gorgonio Pass, the San Andreas fault (SAF) system forms a large left step-over, or restraining left bend. This portion of the San Andreas fault is made up of a complex system of right-lateral thrust oblique-slip faults (Yule and Seih, 2003; Heermance and Yule, 2017). This restraining bend causes slip rates along the SAF system to slow in the region (McGill et al., 2013; Gold et al., 2015; Heermance and Yule, 2017) and implies that slip is somehow transferred to other fault systems, such as the Eastern California Shear Zone (ECSZ) or the San Jacinto fault (Matti and Morton, 1993; Yule and Sieh, 2003; Cook and Dair, 2011). The potential for a large, through-going rupture on the southern SAF through the San Gorgonio Pass (SGP) is not well established (McGill et al., 2013; Gold et al., 2015, Heermance and Yule, 2017). Understanding the potential for a large SAF system rupture is critical to the nearly 20 million people living in the greater Los Angeles area whose primary water, power and transportation lines would be cut in the event of such an event.

Because the SAF system through the SGP is structurally complex, it is unclear whether the observed slip deficit is owing to very long recurrence intervals for large catastrophic events, or that slip/strain is being transferred to other structures. These could include other less studied strands of the SAF system within the SGP, such as the Garnet Hill strand (Gold et al., 2015), or slip could be shunted to other fault systems, such as the ECSZ by way of structures such as the Pinto Mountain fault. Even if the Pinto Mountain fault (PMF) is not directly taking up slip/strain from the SAF system, it may play a key role in the transfer of slip between the SAF system and the ECSZ (Kendrick et al., 2015).

The PMF is a poorly understood left-lateral strike-slip fault that extends from the Mission Creek drainage in the northern San Gorgonio Pass east, through Morongo Valley to Twentynine Palms, forming the boundary between the Mojave Desert and the Eastern Transverse Ranges provinces (Figure 1; Kendrick et al., 2015, Hopson, 2003). The PMF intersects with the San Andreas Fault system in a similar way as the Garlock fault to the north, and may represent a very similar tectonic feature on the southern end of the SAF, though smaller (Allen, 1957). The PMF is expressed in bedrock traces and Quaternary sediments (Allen, 1957; Bryant, 2000), although scarps in Holocene sediments are rarely observed, particularly on the western end (Matti et al., 1988). A goal of this study is to distinguish Holocene fault scarps from geomorphic features on the active and abandoned alluvial surfaces. Total offset of the PMF, as determined by offset bedrock, is between 16 and 19 km (Kendrick et al., 2015, and references within). The rarity of scarps within Holocene sediments and the seismic quiescence of the PMF could be because the PMF has a long recurrence period and/or low slip rate, and has not ruptured in the last several thousand years or has recently become inactive and is becoming locked by the surrounding faults, primarily those in the ECSZ (Hopson, 1998; Kendrick et al., 2015)

In this study, I present a late Quaternary slip rate for the western PMF, along with detailed mapping of the fault using field geologic mapping in conjunction with a 3D digital elevation model from Structure from Motion (SfM), collected in this study, and a 3D digital surface model from Lidar, available online through OpenTopography (Figure 2; NCALM, 2016). I used in situ ^{10}Be terrestrial cosmogenic nuclide exposure dating in conjunction with regional alluvial fan correlation to calculate my preferred surface age

and constrain a slip rate of ~3 mm/yr using an offset alluvial terrace and bedrock strath contact (Figure 3).

Terrace and fan surfaces like the one studied here are common throughout SGP and the Coachella valley, and likely indicate a significant climatic control on fan formation in the region (Owen et al., 2014). I use this relationship while considering regional fan forming events and correlating the fan surfaces in Big Morongo Canyon to others in the SGP region.

Although the ability to determine the full role of the PMF in facilitating transfer of slip around, rather than through the SGP is beyond the scope of this study, this data fills a gap in information on the slip rate of the western PMF over the last ~87 ka. Understanding the activity level of the western PMF is important for development of realistic rupture models of the SAF restraining bend in the SGP and determination of the potential for large, through-going rupture in the region (Yule and Sieh, 2003; Dair and Cooke, 2009).

GEOLOGIC BACKGROUND

San Andreas Fault System

The southern SAF is characterized by two significant restraining bends in the fault trace. The northern bend, commonly known as the "Big Bend", occurs at the transition between the Coast Range and the western Transverse Range provinces, north of Frazier Park, California (Figure 1, inset map; USGS and CGS, 2006). The southern bend in the SAF occurs in the San Gorgonio Pass (SGP), between the San Bernardino and Coachella valleys, and is significantly more complex than the northern Big Bend (Matti and Morton, 1993; Yule and Sieh, 2003; Heermance and Yule, 2017). This left step in the fault forms a 15 km-wide restraining bend, which results in a zone of oblique collision, and a broadly distributed system of dextral, thrust oblique-slip faults (Figure 1; Yule and Sieh, 2003).

The SAF system in the SGP has a significantly lower slip rate than the SAF system to the northwest and southeast (Cooke and Dair, 2011; McGill et al., 2013; Yule and Seih, 2003). The faulting in SGP accounts for only about 1/2 to 1/4 of the dextral slip measured across the SAF system outside of the pass (Heermance and Yule, 2017; Yule and Sieh, 2003) and, in the northern Coachella Valley, is distributed on the Banning, Mission/Mill Creek, and Garnet Hill strands (Kendrick et al., 2015). Slip on the Banning strand accounts for 4-6 mm/year, leaving 8-12 mm/yr (1/2 to 3/4) to be taken up by the Mission/Mill Creek, Garnet Hill and/or other structures within the SAF system whose slip rates are unconstrained, such as the PMF (Gold et al., 2015; Behr et al., 2010). Much of the plate boundary motion that may be "missing" on the SAF system at this latitude could also be taken up by the San Jacinto fault system or the ECSZ, completely avoiding

the SGP (Yule and Sieh, 2003; Onderdonk et al., 2015). Holocene geologic slip rates on the Mission/Mill Creek strand of the SAF appear to change along strike with a very low rate at the eastern margin of San Gorgonio Pass (Kendrick et al., 2015) increasing to 14-17 mm/yr near Indio, California (Behr et al., 2010). Geodetic data also supports this trend of a slip minima through the SGP (Lindsey and Fialko, 2013). A possible hypothesis to explain this change in rate is slip transfer onto other structures like the Banning strand to the south and/or the Pinto Mountain and Morongo Valley faults to the north.

The Pinto Mountain Fault

The PMF is a ~110 km long east-west trending, left-lateral normal fault that extends from east of Twentynine Palms in the ECSZ, west through the Morongo Valley, Big Morongo Canyon and terminates in the Mission Creek drainage, intersecting the SAF system (Figure 1; Allen, 1957; Matti et al., 1988; Hopson, 1998; Kendrick et al., 2015). The PMF bounds the north side of the Morongo Valley, while the south side of the valley is bounded by the Morongo Valley fault (MVF), which splays off the PMF about 1 km west of Yucca Valley (Hopson, 2003). The formation of the Morongo Valley, an apparent extensional basin, is likely linked to the combined right-lateral shear of the SAF and the clockwise rotation of the Eastern Transverse Ranges (Hopson, 2003). Although timing of slip initiation on the PMF is not well established, the PMF may have formed as clockwise rotation of the Eastern Transverse Ranges initiated, and not before 7.3 Ma, based on deformed sedimentary rocks near Yucca Valley (Hopson, 1998; Hopson, 2003).

The slip history and slip rate of the western PMF are poorly understood, with significant temporal variation likely (Kendrick et al., 2015). The PMF has both left-lateral and dip-slip normal offset in both geological observations and geodetic modeling

(Matti et al., 1992, Hopson, 1998, Meade and Hager, 2005). The total displacement of 16 to 19 km, decreasing to the east is determined from offset crystalline basement rocks (Mesozoic and older) observed to the east of Yucca Valley (Langenheim and Powell, 2009; Kendrick et al., 2015). Of this total slip, approximately 9 km has occurred during the Pleistocene or later (Hopson, 1998). The PMF shows no evidence of being seismically active, but is considered a low activity fault, with evidence of late Quaternary slip (Bryant, 2000; WGCP, 2008; Langenheim and Powell, 2009). Scarps in Holocene deposits exist on the central and eastern portion of the fault, but scarps are mostly concealed by Holocene sediments along the western portion of the fault (Matti et al., 1988; Hopson, 1998). Prominent scarps in late Pleistocene age deposits are present along the PMF within the Morongo Valley, while minor scarps in younger Quaternary deposits are rarely observed and are difficult to distinguish (Matti et al., 1988).

Geologic and modeled slip rate estimates for the PMF are based on poorly constrained ages and range from 1 – 7 mm/yr (Hopson, 1998; Kendrick et al., 2015). Paleoseismic work on the eastern end of the PMF near Twentynine Palms reveals five events during the Holocene and two events in the late Pleistocene with an average recurrence interval of 1200-1680 years (Cadena et al., 2004, 2015). Assuming an average slip per event of ~3 m, similar to what was observed during the 1992 Landers Earthquake, the slip rate for the PMF in this area is estimated to be 1.59 – 1.80 mm/yr (Cadena et al., 2015). Geophysical modeling has also been used to estimate the slip rate for the PMF. Geodetic block modeling with GPS data of the SGP region produces a slip rate of 9.4 +/- 0.9 mm/yr in a left-lateral sense, and 9.2 +/- 1.0 mm/yr in a normal sense on the PMF (Meade and Hager, 2005). Other geophysical models have produced slip

rates on the PMF of 5.1 – 6.3 mm/yr for the western end and ~1.6 mm/yr for the central part of the fault, with the eastern end showing low to unrealistic opposite (right-lateral) slip (Spinler et al., 2010). Kendrick et al. (2015) determine a slip rate of 10 – 12.5 mm/yr for the western PMF based on a 1 – 1.25 km offset of the Mill Creek strand of the SAF by the PMF, and ~100 ka age based on soil development and IRSL dating of a fan sequence abandoned at time of offset by the PMF. Allen (1957) was the first to suggest that the PMF may offset the Mill Creek strand of the SAF, and this model was also adopted by Kendrick et al. (2015). In this model, the offset of the Mill Creek strand by the PMF around 100 ka lead to abandonment of the Mill Creek strand of the SAF system and transfer to the San Bernardino, Banning and Garnet Hill strands, and San Gorgonio Pass Fault Zone, even though the Mill Creek strand is more optimally aligned with plate motion (Kendrick et al., 2015).

The PMF is historically aseismic, or inactive, despite the high seismic activity in the region and immediate vicinity (Hopson, 1998). For example, the PMF exhibited an aseismic nature during both the 1992 M7.3 Landers earthquake sequence and the 1992 M6.0 Joshua Tree earthquake, with no aftershocks attributed to the PMF in either case (Hauksson et al., 1993). Although the southern end of the 1992 Landers Earthquake seismic zone crosses the PMF, both cross section and map view of seismicity reveal that the PMF was not activated at any time during the earthquake sequence (Hauksson et al., 1993; Rymer, 1992).

The geometry of the PMF in relation to the SAF system in the SGP is very similar to that of the Garlock fault and its intersection with the SAF at the Big Bend to the north (Allen, 1957). Both the PMF and the Garlock fault intersect the SAF system where there

is a major compressional bend in the fault zone (Allen, 1957; McGill et al., 2009). The similar geometries between these two fault systems may be the result of similar stress regimes at both bends in the SAF system, and similar regional tectonic regimes that are accommodated by ~E-W trending, left-lateral faulting. The PMF may also play a key role in facilitating the transfer of strain between the SAF system and the ECSZ (Matti and Morton, 1993; Seeber et al., 1995; Kendrick et al., 2015).

Regional Controls on Fan Formation

I focus on the control of climate on alluvial fan formation to identify regional fan forming events in the SGP region. The arid model for alluvial fan formation, which is widely accepted in the southwest United States, proposes that aggradation of alluvial fans coincides with transitions from glacial to interglacial climate conditions, and a reduction in the overall vegetation density that triggers increased soil transport to the valley floors (Bull, 1991; Spelz et al., 2008). With this model, one would expect to see alluvial fan aggradation beginning during the transition from or shortly after a glacial period, and incision of fans occurring well into the interglacial or until the beginning of the following glacial period. This model allows one to assume that conditions controlling fan formation in the study area are the same as those controlling alluvial fan formation throughout the SGP and northern Coachella Valley region. Below I used this assumption to compare alluvial fans in Big Morongo Canyon to those in the Mission Creek drainage and interpret regional fan-forming events.

METHODS

Geologic Mapping and Digital Elevation Model Data Collection

I mapped the geology of the roughly two square kilometer study site at a ~1:6,000 scale (Figure 3). The study area focused on the western PMF located in Big Morongo Canyon, parallel to Big Morongo Canyon Road, also listed as Big Morongo Ranch Road, Morongo Valley, California. In this location, Quaternary sediments and basement rocks of the Mojave Desert-type (Kendrick et al., 2015) are offset by the PMF. Base maps for mapping include both Lidar data, available online through OpenTopography, and a structure from motion (SfM) survey collected as part of this study (Figure 2). I used the 3D surface data from both the Lidar and SfM surveys to determine the extent of geologic units and geomorphic surfaces, as well as the locations of the main trance of the PMF and any additional fault splays not previously identified.

One meter resolution Lidar data was provided by William Cochran at Virginia Tech, collected by the National Center for Airborne Laser Mapping (NCALM), available through OpenTopography (Figure 2; NCALM, 2016). I used this to evaluate overall geomorphic features and determine accurate fault location. To evaluate the landscape at a <1 m resolution, I performed a SfM survey (Figure 2). SfM surveys, even those taken with low cost unmanned aerial vehicle systems, compare well with the accuracy of Lidar surveys (Cook, 2017). I collected images for Structure from Motion (SfM) using an unmanned aerial vehicle (UAV) and camera setup. The UAV used is a Phantom 3 Advance quadcopter flown in a pre-programmed grid. The camera used is a Sony EXMORE 12.4 megapixel with GPS/GLONASS (global positioning system/global navigation satellite system). I placed sixteen ground control points with independently

measured GPS locations at regular intervals over the entire surveyed area. Ground control points are critical for improving both relative and absolute accuracy of SfM data (Cook, 2017). Photos were taken with an approximately 60% – 80% overlap, at an altitude of ~50 m. I processed the photos using Agisoft Photoscan Pro version 1.3.1 build 4030 (64 bit). Approximately 850 photos generated a roughly 0.5 km^2 three-dimensional (3D) modeled surface within the study area.

I subdivided geologic units based on classification used by Kendrick et al. (2015) and Dibblee (1967). I mapped all bedrock as basement rocks of the Mojave type (ggm) and two Quaternary alluvial units subdivided into only two members: Old Alluvium (Qoa) and Young Alluvium (Qa). In addition to geologic mapping, I mapped geomorphic features, primarily incised channels and drainage geometries. In this study, the geomorphic surfaces within the Qoa and Qa units are not separated from the geologic features.

Fault offset

Piercing points are defined by projection of the strath contact (Qoa/ggm) to the fault. I mapped the contact defined by piercing points A-A' within ~10 m of the main splay of the PMF and defined a cone within which the piercing point could be located. Because the bottom of the Qoa riser (strath contact) defined by piercing points B-B' and C-C' is buried by Qa sediments, I mapped a reasonable swath in which the contact could be located and project that into the fault. Offset distances used to calculate slip rates were derived from 10,000 Monte Carlo simulations. Vertical offset was measured by comparing the elevations of the piercing points across the fault.

In Situ Terrestrial Cosmogenic Exposure Dating

To determine the age of the old alluvial surface (Qoa) offset by the PMF, I used in situ terrestrial ^{10}Be cosmogenic nuclide surface exposure dating of boulders. ^{10}Be is produced in minerals at the Earth's surface primarily by way of spallogenic reactions between high-energy particles, derived from interactions with cosmic rays, and the oxygen in quartz. Because ^{10}Be is only produced in this way, its concentration in the quartz within a rock or sediments depends on the amount of time that quartz has been exposed at or near (< 2 m) the surface, the production rate of ^{10}Be (considering factors such as elevation, latitude and shielding) and the decay rate of ^{10}Be (Gold et al., 2015). The production and decay rates of ^{10}Be are known, so by measuring the concentration in quartz bearing clasts or sediments from a surface, the exposure age, or time since abandonment, of a fluvially derived surface can be calculated. However, in addition to production rate and decay rate of ^{10}Be, erosion of clasts and surfaces, as well as inherited ^{10}Be must be considered. Erosion can result in reduction of ^{10}Be concentration, thus making the sample appear younger (Gold et al., 2015). In the above calculation for surface age, erosion rate and decay rate combine as factors decreasing ^{10}Be concentration. In contrast, inherited ^{10}Be (inheritance) increases the overall concentration of ^{10}Be and can make the sample appear too old (Hancock et al., 1999). In a fluvial setting, inheritance includes ^{10}Be accumulated during exhumation from the source and the ^{10}Be accumulated as the sample (boulder or other size) is transported from the source to the deposit (fan surface) (Hancock et al., 1999).

Cosmogenic ^{10}Be exposure dating works well for identifying the depositional age of alluvial surfaces on timescales of 10^3 – 10^5 years (Gold et al., 2015). However, within

the Coachella Valley and surrounding areas, cosmogenic dating techniques have proven challenging. Surface ages appear to "max out", or reach a ^{10}Be-production-rate/surface-erosion-rate steady state around 70 – 100 ka (Matmon et al., 2006; Owen et al., 2014). This means that surfaces that are much older than 100 ka based on other dating techniques can have cosmogenic ^{10}Be exposure ages of only 70 – 100 ka.

I sampled the upper 5 to 8 cm from the top of 6 monzo-granite boulders on the surface of Qoa. The boulders range in height from 14 to 40 cm above the present ground surface (locations shown on Figure 3). Boulders selected were identified as most stable, and as far from surface edge erosion and fault splays as possible, typically located on topographic bars. Sampled boulders showed minimal evidence of surface weathering. I did not sample boulders with evidence of significant erosion or spallation. All boulders on the Qoa surface were relatively low to the ground and did not allow for sampling of boulders with height of >40 cm.

I processed ^{10}Be samples at CSUN laboratories. Initial processing included crushing and sieving of samples to size 250 – 600 micrometers and magnetic separation by S.G. Frantz magnetic separator. Following separation of magnetic minerals, I cleaned and leached all nonmagnetic minerals using hydrochloric acid bath, followed by hydrofluoric/nitric acid etching on rollers to eliminate all but quartz. I then added the Beryllium carrier (^{9}Be spike) to the samples and used ion-exchange chromatography to separate all beryllium from a known mass of quartz. I prepared AMS targets for the samples and sent them to Lawrence Livermore National Laboratory Center for Accelerator Mass Spectrometry where the ^{10}Be concentrations were measured as a ratio to the known ^{9}Be spike.

I calculated boulder exposure ages using the CRONUS-Earth online calculator, version 2.3, 2016 (Balco, 2008), using time-independent production rate of ~4 atoms/gram, scaled for elevation and latitude (Lal et al., 1991; Stone, 2000; Borchers et al., 2016). For these samples, I assumed a 0.0 mm/yr erosion rate and 0.0 atom/gram inheritance, as these values could not be quantified within the scope of this study. Modelling ages in CRONUS online calculator with any erosion rate larger than 0.0025 cm/yr produced unrealistically high exposure ages.

Once I determined the age for each sample, I compared of the height of the boulder top above the present surface to the ^{10}Be age of the boulder to determine if deflation of the Qoa has occurred (Behr et al., 2010). Surface deflation, or surface lowering, occurs when the silt and sand matrix of a surface is eroded away, by aeolian or fluvial processes. This erosion leaves behind a vertically compressed sediment column with overturned gravel and cobbles, and can expose boulders that were buried at time of surface abandonment (Figure 4; Behr et al., 2010). I chose to avoid using cobble size or smaller clasts for the ^{10}Be data set to avoid additional age error from surface deflation.

RESULTS

Geology

Within the map area, I identified three primary geologic units; one bedrock unit, and two alluvial units (Figure 5). The bedrock is Mesozoic and older quartz monzonite to granodiorite and gneissic rocks of similar composition (Dibblee, 1967). I grouped these rock types together and adopt the nomenclature presented by Kendrick et al. (2015), calling this unit granitic and gneissic rocks of Mojave Desert type (ggm).

The alluvial units include old alluvium (Qoa) and young alluvium (Qa). For Qoa and Qa, outcrops reveal cobble and boulder sized clasts in a sandy matrix. Clast-supported alluvium is most common, but matrix-supported strata are also observed. Units Qa and Qoa are distinguished on the basis of their different geomorphology, soil development and weathering. Qoa has orange-brown weathering, abundant boulder bars, and some shallow inset swales. Boulders on this surface are often varnished, and range from slightly to highly weathered, and in some places, are broken up and spalled (Figure 6). Although there is significant soil development on the Qoa surface, it does not appear to be as developed as the oldest soils on the surfaces from the Mission Creek drainage (Kendrick et al., 2015; Owen et al., 2014). Soils on fans in the Mission Creek fan complex are much more red than the soil on Qoa (Kendrick et al., 2015).

Qa has tan weathering, no soil development and is likely Holocene in age. boulder bars are not as common on the surface of Qa (excluding the Big Morongo Canyon active channel). Boulders in Qa have little to no varnish, are slightly to moderately weathered, rarely spalled, and tend to be short or more completely buried than boulders on the Qoa

surface (Figure 6). The Qa surface appears to have no deflation, with some shallow gullies from recent water flow.

Fault Outcrops and Pleistocene Offset

The main splay of the PMF is expressed as a prominent scarp in late Pleistocene alluvial sediments (Qoa) in Big Morongo Canyon, on the northwest side of the Morongo Valley (Figure 2 and 3). I observed no scarps along the main splay of the fault in Qa either in the field or in Lidar and SfM data. The main splay of the PMF strikes N85°E to due E-W in the study area. Where the main splay outcrops in a road cut orthogonal to the fault, I observed that the fault zone is approximately 8-10 m wide, with near vertical to slightly north dip (Figure 7). In this exposure, the fault juxtaposes ggm and Qoa. Although the roadcut shows down-to-the-north separation across the fault zone, this is due to primarily left-lateral offset of a gently east-dipping unit Qoa such that originally lower elevation Qoa is now juxtaposed against originally higher elevation ggm (beneath Qoa). The elevations of offset piercing points support almost pure strike-slip motion (described below). Logging of this outcrop revealed two main fault planes that bound tectonically mixed material between them, including large crushed displaced bedrock clasts and fault gouge with mixed alluvium/colluvium. The bedrock in this outcrop is crushed, but exhibits a unique sub-vertical sheared fault gouge.

Roughly 80 m to the north of the main splay of the PMF on the eastern side of the study area, a second, previously unidentified fault splay outcrops in another road cut. This splay bounds the northern side of a shutter ridge that blocks a beheaded stream channel in the eastern portion of Figure 3. Observation of the fault outcrop in the road cut reveals a roughly 1 m wide fault zone, with a near vertical dip. In this outcrop the fault

juxtaposes units ggm and Qoa, with a down-to-the-south separation that again is probably due primarily to sinistral offset of uneven topography (Figure 8). The fault outcrop has several localized subvertcal shear planes, but within a much narrower zone than the main fault splay to the south (Figure 9).

Offset values of the PMF are summarized in Table 1. Along the main splay of the PMF, I identified two sets of offset piercing points. The first piercing points, A-A' (Figure 3), are defined by the projection of the western edge of the contact between the Qoa and ggm (strath) to the main strand of the PMF. The piercing points are left-laterally offset by a map distance of 188 – 214 m. The elevation differences indicate a down-to-the-south vertical offset of ~10 m (961 m on N vs 951 m on S). The sinistral strike-slip to dip-slip motion is thus about 20:1. The excellent exposure and high angle of intersection of this contact with the fault makes this the best constrained offset across the PMF.

The second offset, piercing points B-B' (Figure 3), represents the truncations of the eastern edge of the Qoa/ggm contact (strath) by the fault. The piercing points are left-laterally displaced by map distance of 251 – 300 m. The elevation differences indicate a down-to-the-south vertical displacement of ~7 m (949 m on N and 942 m on S), giving a similar but slightly higher strike-slip to dip-slip ratio for fault motion. Offset B-B' is not as well constrained as A-A' because the contact is buried by unit Qa to the north of the fault. Rates for both offsets are presented below.

I mapped three to four additional, previously unidentified discontinuous fault splays, north of the main splay, on the western side of the study area. These splays produce scarps within Qoa sediments, but these scarps do not extend into Qa. These scarps strike roughly N70°E. Here, the buried Qoa/ggm contact (strath) is left-laterally

offset across two of these splays by 40 – 89 m (C-C' on Figure 3). Because this is the same contact offset at A-A' and B-B', I consider this additional offset to the offset measured on the main splay of the PMF. For the western PMF, I determined a total offset of 228 – 303 m (for A-A' plus C-C') or 291 – 389 m (B-B' plus C-C').

Holocene Fault Offset

The northern fault splays on the western side of the study area do no exhibit scarps in Qa sediments, but do have evidence of recent, possibly Holocene offset. A channel incised into Qoa by 5 – 7 m is left-laterally offset by a total of 23 – 38 m across two fault splays (D-D' on Figure 3). This incised channel is not offset by the main splay of the PMF (Figure 10). Although I cannot directly constrain the age of this incision, I interpret this offset as younger than the offset of the Qoa/ggm strath contact, and I did not include it in the long-term slip rate calculation. It is likely that this incision occurred following the termination of the last glacial maximum around ~18 ka (Jouzel et al., 1993; Petit et al., 1999), and could be as young as the Holocene.

In addition to the scarps I mapped in Qoa on the western side of the study site, I identified a subtle escarpment that appears to be a westward continuation of the northern splay observed in outcrop on the north side of the Qoa surface, into the Qa surface (Figure 3). This escarpment is 0.5 – 1 m high and strikes roughly parallel to the main splay of the PMF at N85°E (Figure 11). Within Qa, I did not measure any horizontal offset along this escarpment. This escarpment continues for about 200 m to the west before projecting into an area modified by earth-moving equipment for presumed fire and flood control. Expression of this scarp appears again to the west of the modified area, juxtaposing ggm/Qoa with Qa. This escarpment runs parallel to and within about 5 – 10

m of a small road feature, suggesting the escarpment may be the result of recent anthropogenic surface modification. However, the escarpment is bounded on either side by mature vegetation, including >2 m-tall yucca, cholla, and bushes. With the SfM 3D surface model, I mapped the extent of modification, and find that the fault splay is outside of that modification in this area (Figure 12). Stream flow in this part of the study area can also run parallel to the escarpment. However, I observed similar soil development on both sides of this escarpment, which suggests that the now offset sides were part of the same surface, rather than the incision and deposition of a new terrace. Additionally, I compared the sinuosity of the escarpment to that of the fluvial gullies throughout the Qa and Qoa surface and see that the escarpment has a significantly lower sinuosity (Figure 13). A tectonic origin for the escarpments is therefore most likely.

Geochronology

I sampled six boulders from Qoa (Figure 3, Figure 14). Concentrations of ^{10}Be for these samples ranges from 4.4 x 10^5 atoms/gram to 6.4 x 10^5 atoms/gram. Results of the CRONUS-Earth online calculator are given in Table 2. I calculated production rate ages using CRONUS Earth online calculator version 2.3 (Balco 2008). Exposure ages for the six boulder samples from the surface of Qoa range from 62.7 +/- 5.6 ka to 88.2 +/-7.9 ka, assuming zero inheritance and zero erosion rate.

I plotted the boulder ages versus the height of the top of the boulder above the surface of Qoa (Figure 15), and observe a trend that suggests some deflation of the Qoa surface has occurred. The three boulders with the youngest exposure ages (PMF-16-02, PMF-16-01 and PMF-16-04) are the three shortest boulders (< 30 cm). The data points for these three samples form a steep slope correlating young ages with short heights of

boulders, indicating that the youngest/shortest sample has been exhumed most recently (Figure 15; Behr et al., 2010). This suggests that deflation of the Qoa surface has occurred, and those boulders shorter than 30 cm were buried at the time of surface abandonment, and were exhumed later, once the surface began to deflate. For samples from boulders at or above the height of 30 cm (PMF-16-03, PMF-16-05 and PMF-16-06), the slope of data points is roughly horizontal and the age errors overlap (Figure 15). This near horizontal slope indicates that all boulder tops above 30 cm have not experience differential exposure, and have been exposed at the surface since the time of abandonment. The ages of these three boulders should represent the true exposure age of the surface of Qoa. Therefore, I used only the exposure ages from samples PMF-16-03, PMF-16-05 and PMF-16-06 to calculate a weighted average ^{10}Be exposure age with one standard error of 86.9 +/- 4.5 ka for the surface of Qoa.

Although I cannot determine the exact age of Qa sediments, I interpret a Holocene age based on the lack of soil development and unaltered nature of boulders on its surface (Figure 5, Figure 6).

Slip Rates

I calculated the slip rate for the western PMF using offset derived from 10,000 Monte Carlo simulations. Parameters used in the simulation are presented in Table 1. I calculated slip rates for the main splay of the PMF with offsets A-A' and B-B' and slip rates for all splays of the PMF by adding the slip rate of C-C' to both A-A' and B-B' slip rates. Histograms of the slip rate Monte Carlo simulation are shown in Figure 16. Using the weighted mean age of 86.9 +/- 4.5 ka for the Qoa surface, I calculated slip rates with one standard error of 3.0 +0.6/-0.4 mm/yr for the offset of A-A' plus C-C', or 3.9 +0.6/-

0.5 mm/yr for the offset of B-B’ plus C-C’ (see discussion below for offset uncertainties and slip rate implications).

The offset channel incised into the Qoa surface also provides an opportunity to speculate on a more recent slip rate for the western PMF. Assuming incision occurred following the last glacial maximum, between 10 and 20 ka, I calculated a slip rate of 1.1 – 3.7 mm/yr for the last 10-20 ka. This slip rate overlaps with the calculated slip rate based on offsets of the Qoa/ggm strath contact.

DISCUSSION

Geochronology Uncertainties

Because I know that the surface of Qoa has experienced deflation, I chose the three oldest ages that have not been affected by deflation (Figure 15) to calculate a weighted mean age of 86.9 +/- 4.5 ka for the surface of Qoa, assuming zero inheritance and zero erosion of boulder tops. I was not able to quantify the amount of inherited ^{10}Be in the boulders on surface Qoa within the scope of this study. However, Big Morongo Canyon is narrow with significant surrounding relief and the samples are compositionally consistent with the exposed bedrock of those peaks. Thus, I assume that the amount of time between initial exhumation and final deposition of the sampled boulders is short, resulting in inheritance on the order of ~1.0 ka, which is reasonable for the alluvial system in the study area (McGuire, 2011) and falls well within the age error.

I consider the ^{10}Be exposure age of Qoa a minimum age because I did not include erosion of the boulder tops in the age model. Erosion of a boulder surface prior to sampling will result in loss of accumulated ^{10}Be, reducing total concentration and resulting in an exposure age for the boulder that is too young. I was not able to constrain an erosion rate within the scope of this study, and thus assume 0.0 mm/yr erosion rate. However, I know that this is not the case, and that boulders have experienced some erosion, particularly given their old age. Therefore, present 86.9 +/- 4.5 ka as the minimum age for the surface of Qoa.

In the SGP/northern Coachella Valley region, local erosion rates have resulted in ^{10}Be accumulation reaching a maximum value around 70 – 100 ka, as production rate and decay plus erosion rate reach an equilibrium (Matmon et al., 2006; Owen et al., 2014;

Kendrick et al., 2015). Boulder ages from the Qoa surface fall into this age range and for this reason it is important to consider regional controls on fan building, and the possibility of localized fan forming events that can be compared between fan complexes.

Regional Correlation of Surfaces

I compared alluvial surfaces in Big Morongo Canyon and their ages to those of the nearby Mission Creek fan complex. The Mission Creek alluvial fan complex, located in the Mission Creek drainage at the eastern end of the San Bernardino Mountains, is a complex of several fan surfaces, whose deposition spans a significant amount of time during the late Pleistocene (Kendrick et al., 2015). The precise timing of deposition and abandonment of the fan complex has been a point of contention (Owen et al., 2014; Kendrick et al., 2015). Dating methods such as cosmogenic ^{10}Be have provided controversial ages, but infrared stimulated luminescence (IRSL) have proven more successful (Kendrick et al., 2015). I adopt the nomenclature used by Owen et al. (2014) for the fan surfaces but include data from both Owen et al. (2014) and Kendrick et al. (2015) in the discussion.

Figure 17 is a schematic topographic profile of terrace levels in the northwestern Coachella and Morongo valleys. Age data from both Owen et al. (2014) and Kendrick et al. (2015) are shown for the dated surfaces. Within the Mission Creek complex, the two oldest surfaces, FM1 and FM2 sit ~200 m and 40 m above the present active channel and have ^{10}Be ages of ~68 ka and ~86 ka respectively (Owen et al., 2014). These ages are out of stratigraphic order, as FM2 is incised deeply (>100 m) into FM1, and should therefore be younger (Figure 17). Additionally, soil development suggests that surfaces FM1 and FM2 are around 500 ka and >250 ka respectively, which contradicts both relative and

precise ages presented by Owen et al. (2014) (Kendrick et al., 2015). It is possible that surfaces FM1 and FM2 have reached the ^{10}Be secular equilibrium, or have experienced significant erosion and deflation. There are no fan surfaces in Big Morongo Canyon that are comparable to the FM1 and FM2 fan surfaces.

I believe that, based on height above active channel, age and relative soil development, the FM4 surface within the Mission Creek fan complex is the fan surface most comparable to the Qoa surface in Big Morongo Canyon. FM4 sits 15 – 20 m above the active channel and has a ^{10}Be age of ~68 ka (Owen et al., 2014). This age is of concern in that it is the same as the FM1 surface, ~170 m above (Figure17). IRSL ages for the sediments below the surface of FM4 produce an age range of 95 – 106 ka (Kendrick et al., 2015). Because the ^{10}Be age for surface FM4 is the same as FM1, and suggests that this surface has also reached ^{10}Be secular equilibrium, I accept the IRSL age of 95 – 106 ka as the preferred minimum age for the surface of FM4. I believe that the same regional fan forming event responsible for FM4 is responsible for formation of Qoa in Big Morongo Canyon.

Surfaces FM5, FM6 and FM7 in the Mission Creek fan complex are comparable to the Qa sediments and surfaces, and represent a Holocene fan formation and incision (Figure 17). I did not subdivide Qa into surfaces within the scope of this study, and cannot directly compare Holocene surfaces between Big Morongo Canyon and the Mission Creek fan complex.

The timing and regional span of the late Pleistocene and Holocene fan forming events suggest climate was the dominant control (Owen et al., 2014). Based on the arid model for alluvial fan formation, fans aggrade as the global climate warms (Bull, 1991;

Spelz et al., 2008). I believe that Qoa and FM4 began to aggrade following the penultimate glacial maximum, as the global climate transitioned from glacial to interglacial conditions. Regional abandonment and incision of alluvial surfaces occurred between 80 – 110 ka.

Fault Scarps

The main splay of the PMF in this study area is clearly visible cutting Qoa sediments, and can be easily identified in the field (Figure 2). Lidar and SfM data helped identify additional subtle scarps in both Qoa and Qa sediments that had not previously been recognized. The main splay of the PMF does not produce scarps in the surface of Qa and does not offset a modern channel incised into the Qoa surface (Figure 10), and thus has likely not ruptured since this incision event. However, I observed scarps within Qa sediments and offset of the modern channel by the northern splays of the PMF (Figure 3). The northern splays of the western PMF has therefore ruptured since the incision of unit Qa. Though the age of Qa and its incision are not known in Big Morongo Canyon, rupture of the western PMF must post-date 3-8 ka if correlations with Qa and FM5-7 in the Mission Creek fan complex are valid.

It is noteworthy that the main splay of the western PMF does not appear to cut unit Qa. The main splay of the PMF is characterized by a striking, linear scarp in Qoa, whereas the northern splays have subtle scarps and form en echelon steps. The discontinuous northern splays may be a new fault trace that has developed as the more prominent main splay has been abandoned. Without paleoseismic trench data for the western PMF, I cannot determine if all splays in the system rupture together, or if slip tends to partition between the northern splays and the main splay during an earthquake.

Offset Uncertainties

Within the study area, I identified dominantly sinistral offset with a <5% down-to-the south vertical component. Matti et al. (1992) recognized normal dip-slip separation, but I did not observe any significant component of dip-slip in the study area. Apparent normal separation observed in the fault outcrops (Figure 7 and Figure 8) is primarily an artifact of left-lateral slip juxtaposing a stratigraphically higher (Qoa) and lower (ggm) units.

Piercing points of offset features along the main splay can be pinpointed in the field and on structure from motion data, and generally have low uncertainties, even where the contact (strath) is buried by a thin layer of Qa. Offset A-A' on the main splay of the western PMF is the best constrained at 188 – 214 m. An additional offset of 40 – 89 m is measured on the northern splays (C-C'). Offset B-B' is 251 – 300 m and is significantly greater than A-A'.

The discrepancy between A-A' and B-B' is intriguing and can be explained by two models. After initial fault offset, erosion of the downstream portion of the eastern margin of paleo channel would produce a greater offset value for B-B'. This erosion can explain why Qa is not present to the south of the fault. Alternatively, the larger B-B' displacement can be explained by an earlier age for abandonment of the eastern channel margin as sinistral motion across the fault moved the shutter ridge into the paleochannel. For this model the western channel margin remains active for some time after the eastern margin is abandoned and presumably shielded by the shutter ridge. Reconstructions for the various offsets of the western PMF in the study area is shown in Figure 18.

Motion across the northern fault scarp is constrained by 23-38 m of sinistral offset of a terrace riser, D-D' in Figure 19. Although the geomorphology of this incised channel is complicated by high sinuosity, D-D' may record displacement during some or all of the 5 – 7 rupture events since the latest Pleistocene on the eastern end of the PMF (Cadena et al., 2015). I do not know the timing of incision of the channel into Qoa, and know only that the base of the channel contains Qa sediments. Using the slip rate determined for the PMF system, I estimated the time of incision based on total offset of the channel. Based on the offset of 23 – 38 m and a slip rate of 3.0 +0.6/-0.4 mm/yr, incision likely occurred between 6,389 years b.p. and 14,615 years b.p. This age is consistent with Holocene incision events that have been documented elsewhere in the northern Coachella Valley (Figure 17; Heermance and Yule, 2017).

Tectonic Implications

There are several characteristics and interpretations for the Garlock fault that are, or may be similar to the PMF. Both the Garlock fault and the PMF have evidence of Holocene slip, although Holocene offsets along the western PMF are more subtle (Matti et al., 1992; McGill et al., 2009). It is proposed that a combination of compressional forces moving the Mojave block to the northeast, rotation of the Mojave block, and differential extension of the Basin and Range cause left-lateral slip on the Garlock fault (McGill et al., 2009). The PMF may help accommodate compression occurring within the SGP, or transtension of the ECSZ, but rotation in the region likely has a significant role in the formation of the PMF (Hopson, 2003). The PMF is the northern boundary of the clockwise rotating Eastern Transverse Ranges province, and the southern boundary of the clockwise rotating Mojave block (Hopson, 2003). It is possible that the PMF is

accommodating the rotation in much the same way that the Garlock fault could accommodate rotation (Hopson, 2003).

The region around the Garlock and Pinto Mountain faults is dominated by NW trending strain accumulation within the Walker Land and ECSZ, with little to no strain accumulating in the E-W to NE-SW direction (McGill et al., 2009). Geodetic data collected from 1992 – 2000 showed strain accumulation concentrated on the Blackwater and Little Lake fault zones, which cross the Garlock fault and roughly connect the 1872 Owens Valley earthquake to the 1992 Landers rupture, with little to no strain accumulation on the Garlock fault (McGill and Rockwell, 2003). Similarly, the PMF has been historically aseismic, despite the 1992 Joshua Tree earthquake and the adjacent 1992 Landers earthquake whose epicenters are immediately south and north of the PMF, respectively (Hauksson et al., 1993; Rymer, 1992). The recent inactivity and lack of strain accumulation on the PMF and Garlock fault, could support an oscillatory pattern between activity on NW-SE trending right-lateral fault systems (ECSZ, Walker Lane) and EW to NE-SW trending left-lateral fault systems (PMF and Garlock fault) (McGill and Rockwell, 2003). This oscillatory pattern would accommodate observed the rotation of the Mojave and Eastern Transverse Ranges blocks (Hopson, 2003).

The precise interaction between the SAF system and the western PMF remains equivocal. Much as the Garlock fault appears to be an accommodating structure, I believe that the PMF serves a similar purpose, accommodating rotation or differential slip between the San Gorgonio Pass and Mission Creek strands of the SAF and the Coachella Valley strand of the SAF to the south. Additional geologic and geodetic study of the PMF is necessary to define this relationship.

Slip Rate Implications

In this study, I determined a late Quaternary slip rate of 3.0 +0.6/-0.4 mm/yr or 3.9 +0.6/-0.5 mm/yr for the western PMF. The different rates reflect a difference in late Pleistocene offsets A-A' and B-B' (Figure 3 and 18). I prefer the lower rate because the A-A' offset is best constrained and the B-B' is ambiguous. Ultimate resolution of this discrepancy will require age dating of unit Qa and trench exposures to better constrain the location of the possible buried strath along the eastern paleochannel near 'B' (Figure 3).

The ~3 mm/yr slip rate is the maximum long term slip rate, because I considered the cosmogenic ^{10}Be age of 86.9 +/- 4.5 ka to be the minimum surface exposure age. This slip rate is higher than the 1.5-1.8 mm/yr determined from a paleoseismic study on the eastern PMF (Cadena et al., 2015), but significantly lower than the 5-9.2 mm/yr geodetically determined slip rates (Meade and Hager, 2005; Spinler et al., 2010;) and the 10-12.5 mm/yr slip rate determined from interpretations of Mission Creek fan complex formation (Kendrick et al., 2015). I calculated a long-term slip rate for the western PMF, and am not able to account for temporal variability because I used only one feature offset by the fault to determine the slip-rate. To better constrain temporal slip rate variations for the western PMF, additional, independent features offset by the fault or the age of basal sediments ponded above the beheaded channel (Qa) are necessary.

Significant temporal variation in the slip rate and activity level of this fault would have a large effect on the hazard of this fault and the likelihood of a large rupture. The PMF may have a complex relationship with adjacent faults in the ECSZ, which may complicate the evaluation of hazard even more. Assuming an average horizontal offset of 3-4 m during a significant rupture, similar to the 1992 Mw 7.3 Landers rupture (SCEDC,

2013), a slip rate of 3.0 +0.6/-0.4 mm/yr would produce a rupture every 1000 – 1300 years. The average recurrence interval for the eastern end of the PMF is 1200 – 1500 for the last ~9 ka (Cadena et al., 2015). Paleoearthquake data for the western PMF is needed to establish whether recurrence occurs periodically, irregularly or is controlled by regional stress changes within the ECSZ or SAF system.

CONCLUSIONS

I determined the minimum cosmogenic ^{10}Be surface exposure age of 86.9 +/- 4.5 ka for an alluvial surface offset by the western PMF in the Morongo Valley. This age is consistent with a regional, climatically controlled fan building following the penultimate glacial maximum. I measured 188 – 214 m and 251 – 300 m of left-lateral offset on the main splay, with an additional 40 – 89 m of offset on previously unidentified northern fault splays. Using the preferred sum of 188 – 214 m plus 40 – 89 m of offset, I calculated a slip rate of 3.0 +0.6/-0.4 mm/yr for the western PMF over the last ~87 ka. This geologic slip rate is significantly lower than other geologic rates for the western PMF and geodetically modeled slip rates, but is slightly faster than geologic rates estimated from paleoearthquakes on the eastern end of the fault. Determining the age of the base of the Qa unit ponded on the north side of the PMF is critical for pinpointing the completion of beheading of the paleochannel (B-B'), thus better constraining temporal variation in slip rate.

The western PMF in the study area is made up of several splays, which include the previously mapped main splay with scarps in Pleistocene sediments and a series of subparallel, discontinuous splays to the north of the main splay, with scarps in both Pleistocene and Holocene sediments. Although it appears that the northern splays of the PMF ruptured most recently, it is likely that the PMF is capable of rupturing all splays simultaneously, similar to the 1992 Landers rupture. A deep but narrow channel incised into the Qoa surface is left-laterally offset by two of the northern splays mapped in this study, but is not horizontally offset by the main splay of the PMF. Based on the slip rate calculated for the PMF system and the offset distance I calculated an incision age of 6.4 –

14.6 ka, which is consistent with climatically controlled regional incision in the Holocene, which has been observed elsewhere in the northern Coachella Valley.

Although the PMF has been historically aseismic, the geologic slip rate and Holocene offset suggest that this fault is a recently active fault, capable of significant rupture every ~1.3 ka. The earthquake recurrence may be complicated, however, by a complex relationship with surrounding faults. The PMF is similar to the Garlock fault in its geometry with the SAF, and could play a similar role in the overall tectonic regime by accommodating rotation of the Mojave block to the north and the eastern Transvers Range block to the south. A possible oscillatory relationship observed between the ruptures on the Garlock fault and ruptures in the ECSZ could also exist between the PMF and the ECSZ and/or the SAF. The exact relationship between the PMF and the SAF and ECSZ remains equivocal, particularly without paleoseismic data for the central and western PMF. However, the PMF has been active in the Holocene, and thus may play an important role in the seismic hazard of southern California, driving the need for continued research of the PMF.

REFERENCES CITED

Allen, C.R., 1957, San Andreas fault zone in San Gorgonio Pass, southern California: Geological Society of America Bulletin, v. 68, p. 315-350, doi:10.1130/0016-7606(1957)68[315:SAFZIS]2.0.CO;2.

Armstrong, P.A., Perex, R., Owen, L.A., Finkel, R. C., 2010, Timing and controls on late Quaternary landscape development along the eastern Sierra El Mayor rang front in northern Baja California, Mexico: Geomorphology, vol. 114, pp. 415-430, doi:10.1016/j.geomorph.2009.08.005.

Balco, G., Stone, J.O., Lifton, N.A., Dunai, T.J., 2008, A complete and easily accessible means of calculating surface exposure ages or erosion rates from ^{10}Be and ^{26}Al measurements: Quaternary Geochronology, vol. 4, p. 93-107.

Balco, G., Briner, J., Finkel, R., Rayburn, J., Ridge, J., Scheafer, J., 2009, Regional beryllium-10 production rate calibration for late-glacial northeastern North America: Quaternary Geochronology, v. 4, is. 2, p. 93-107.

Behr, W.M., Rood, D.H., Fletcher, K.E., Guzman, N., Finkel, R., Hanks, T.C., Hudnut, K.W., Kendrick, K.J., Platt, J.P., Sharp, W.D., Weldon, R.J., Yule, J.D., 2010, Uncertainties in slip-rate estimates for the Mission Creek strand of the southern San Andreas fault at Biskra Palms Oasis, southern California: GSA Bulletin, v. 122, no. 9/10, p. 1360-1377.

Blisniuk, K., Scharer, K., Sharp, W., Burgmann, R., Raymer, M., Rockwell, T., and Williams, P., 2012, Rapid late Quaternary slip on the San Andreas fault zone in the Coachella Valley and the distribution of slip across the Pacific-North American plate boundary, AGU Fall meeting, San Francisco, CA.

Borchers. N., Marrero, S., Balco, G., Caffee, M., Goehring, B., Lifton, N., Nishiizumi, K., Phillips, F., Shaefer, J., Stone, J., 2016, Geological calibration of spallation production rates in CRONUS-Earth project: Quaternary Geochronology, vol. 31, p. 188-198.

Bryant, W.A., compiler, 2000, Fault number 118, Pinto Mountain fault zone (includes Morongo Valley fault) in Quaternary Fault and Fold Database of the United States: U.S. Geological Survey, http://earthquakes.usgs.gov/hazards/qfaults (accessed October 2015).

Bull, W.B., 1991, Geomorphic Responses to Climate Change, Oxford University Press, New York.

Cadena, A.M., Rubin, C.M., Rockwell, T.K., Walls, C., Lindvall, S., Madden, C., Khatib, F., and Owen, L., 2004, Late Quaternary activity of the Pinto Mountain fault at the Oasis of Mara: Implications for the Eastern California Shear Zone: Geological Society of America 2004 Annual Meeting, Abstracts with Program, vol. 36, no. 5, p. 137.

Cadena, A., Rockwell, T., Rubin, C., Lindvall, S., Walls, C., and Madugo, C., 2015, Paleoseismic evidence for Holocene activity on the Pinto Mountain fault, Southern California Earthquake Center Fall 2015 Annual Meeting Abstract (Poster 113).

Cook, K.L., 2017, An evaluation of the effectiveness of low-cost UAVs and structure from motion for geomorphic change detection: Geomorphology, v. 278, p. 195-208.

Cooke, M., and Dair, L., 2011, Simulating the recent evolution of the southern big bend of the San Andreas fault, Southern California: Journal of Geophysical Research, v. 116.

Dibblee, T.W., Jr, 1967, Geologic map of the Morongo Valley quadrangle, San Bernardino and Riverside Counties, California: U.S. Geological Survey Miscellaneous Geologic Investigations Map I-517, scale 1:62,500.

Gold, P., Behr, W., Rood, D., Sharp, W., Rockwell, T., Kendrick, K., Salin, A., 2015, Holocene geologic slip rate for the Banning strand of the southern San Andreas Fault, southern California: Journal of Geophysical Research: Solid Earth, 120.

Hancock, G.S., Anderson, R.S., Chadwick, O.A., Finkel, R.C., 1999, Dating fluvial terraces with ^{10}Be and ^{26}Al profiles: application to the Wind River, Wyoming: Geomorphology, v. 27, p. 41-60.

Hauksson, e., Jones, L.M., Hutton, K., and Eberhard-Phillips, D., 1993, The 1992 Landers Earthquake sequence: Seismological observations: Journal of Geophysical Research, v. 98, p.19,835-19,858, doi:10.1029/93JB02384.

Heermance, R.V., Yule, J.D., 2017, Holocene slip rates along the San Andreas Fault System in the San Gorgonio Pass and implications for large earthquakes in southern California: Geophysical Research Letters (In Press).

Heisinger, B., Lal, D., Jull, A.J.T., Kubik, P., Ivy-Ochs, S., Neumaier, s., Knie, K., Lazarev, V., Nolte, E., 2002a, Production of selected cosmogenic radionuclides by muons: 1. Fast muons: Earth and Planetary Science Letters, v. 200(3-4), p. 345-355.

Heisinger, B., Lal, D., Jull, A.J.T., Kubik, P., Ivy-Ochs, S., Knie, K., Nolte, E., 2002b, Production of selected cosmogenic radionuclides by muons: 2. Capture of negative muons: Earth and Planetary Science Letters, v. 200(3-4), p. 357-369.

Hopson, R.F., 1998, Quaternary geology and neotectonics of the Pinto Mountain Fault, Mojave Desert, southern California: California Geology, v. 51, no. 6, p. 3-13.

Hopson, R.F., 2003, The origin of Morongo Valley, an extensional basin in the Eastern Transverse Ranges, southern California: Geology of the Mojave Desert and Adjacent Terranes: Published for NAGT-FWS 2003 Spring Conference, 21-23 March 2003, Chaffey College. National Association of Geoscience Teachers, Far Western Section, 2003.

Jouzel, J., Barkov, N.I., Barnola, J.M., Bender, M., Chappellaz, J., Genthon, C., Kotlyakov, M.V., Lipenkov, V., Lorius, C., Petit, R., Raynaud, D., Raisbeck, G., Ritz, C., Sowers, T., Stievenard, M., Yiou, F., Yiou, P., 1993, Extending the Vostok ice-core record of the palaeoclimate to the penultimate glacial period: Nature, v. 364, p. 407-412, doi:10.1038/364407a0.

Kendrick, K.J., Mattie, J.C., Mahan, S.A. 2015, Late Quaternary slip history of the Mill Creek strand of the San Andreas Fault in San Gorgonio Pass, southern California: The role of subsidiary left-lateral fault in strand switching: GSA Bulletin, v. 127, no. 5/6, p. 825-849.

Lal, D., 1991, Cosmic ray labeling of erosion surfaces: in situ nuclide production rates and erosion, Earth and Planetary Science Letters, vol. 104, p. 424-439.

Langenheim, V.E., Powell, R.E., 2009, Basin geometry and cumulative offsets in the Eastern Transverse Ranges, southern California: Implications for transrotational deformation along the San Andreas fault system: Geosphere, v. 5, no. 1, p. 1-22, doi:10.1130/GES00177.1.

Linsey, E.O., Fialko, Y., 2013, Geodetic slip rates in the southern San Andreas Fault system: Effects of elastic heterogeneity and fault geometry: Journal of Geophysical Research, col. 118, iss. 2, p. 689-697.

Matmon, A., Nichols, K., Finkel, R., 2006, Isotopic insights into smoothening of abandoned fan surfaces, Southern California; Quaternary Research, v. 66, p. 109-118.

Matti, J.C., Carson, S.E., Kilburn, J.E., Briscom, A., Kuizon, L., and Prose, D., 1988, Mineral Resources of the Morongo Wilderness Study Area (CDCA-218), San Bernardino County, California: U.S. Geological Survey Bulletin 1710-B, 34 p.

Matti, J., Morton, D., Cox, B., 1992, The San Andres fault system in the vicinity of the central Transverse Ranges province, southern California, U.S. Geological Survey Open File Report 92-354, 40pp.

Matti, J., and Morton, D., 1993, Paleographic evolution of the San Andreas fault in southern California: A reconstruction based on a new cross-fault correlation, in

Powell, R., II, and Matti, J., eds., The San Andreas fault system: Displacement, palinspathic reconstruction and geologic evolution: Geological Society of America Memoir 178, p. 107-159.

McGill, S., Owen, L., Weldon, R., Kendrick, K., 2013, Latest Pleistocene and Holocene slip rate for the San Bernardino strand of the San Andreas fault, Plunge Creek, Southern California: Implications for strain partitioning within the southern San Andreas fault system for the last ~35 k.y.: GSA Bulletin, v. 125, no. 1/2, p. 48-72.

McGill, S., Wells, S., Fortner, S., Kuzman, H., McGill, J., 2009, Slip rate of the western Garlock fault, at Clark Wash, new Lone Tree Canyon, Mojave Desert, California: GSA Bulletin, vol. 121, no. 3/4, p. 536-554.

McGill, S.F., Rockwell, T.K., 2003, Irregular recurrence of paleoearthquakes along the central Garlock fault near El Paso Peaks, California: Journal of Geophysical Research, v. 108, n. B7, p. 2356, doi:10.1029/2001JB001744.

McGuire, K.E., 2011, Tracking Cosmogenic ^{10}Be in multiple grain sizes down an alluvial system in an active orogen, [Master's thesis]: California State University, Northridge, 123 p.

Meade, B.J., and Hager, B.H., 2005, Block models of crustal motion in southern California constrained by GPS measurements: Journal of Geophysical Research, v. 110, p. B03403, doi:10.1029/2004JB003209.

NCALM (National Center for Airborne Laser Mapping), 2016, San Bernardino Mountains, CA 2016; OpenTopography, compiler doi: 10.5069/G9SX6B51, http://opentopo.sdsc.edu/datasetMetadata?otCollectionID=OT.052017.32611.1 (accessed July, 2017).

Onderdonk, N.W., McGill, S.F., Rockwell, T.K., 2015, Short-term variations in slip rate and size of prehistoric earthquakes during the past 2000 years on the northern San Jacinto fault zone, a major plate-boundary structure in southern California: Lithosphere, v. 7, mo. 3, p. 211-234.

Owen, L.A., Clemmens, S.J., Finkel, R.C., Harrison, G., 2014, Late Quaternary alluvial fans at the eastern end of the San Bernardino Mountains, southern California: Quaternary Science Reviews, vol. 87, pp. 114-134.

Petit, J.R., Jouzel, J., Raynard, D., Barkov, N.I., Barnola, J.M., Basile, I., Benders, M., Chappellaz, J., Davis, M., Delaygue, G., Delmotte, M., Katlyakov, V.M., Legrand, M., Lipenkov, V.Y., Lorius, C., Pepin, L., Ritz, C., Saltzman, E., Stievenard, M., 1999, Climate and atmospheric history of the past 420,000 years from the Vostok ice core, Antarctica; Nature, v. 399, p. 429-436.

Rymer, M., 1992, The 1992 Landers Earthquake and surface faulting, Earthquakes and Volcanoes, v. 23, no. 5, pp. 209-2018.

SCEDC (Southern California Earthquake Data Center), 2013, Landers Earthquake: Southern California Earthquake Center, Caltech, http://scedc.caltech.edu/significant/landers1992.html, doi:10.7909/C3WD3Xh1, (accessed July, 2017).

Seeber, L., Armbruster, J.G., 119, The San Andreas Fault system through the Transvers Ranges as illuminated by earthquakes: Journal of Geophysical Research, vol. 100, no. B5. P. 8285-8310.

Spelz, R.M., Fletcher, J.M., Owen, L.A., Caffee, M.W., 2008, Quaternary alluvial-fan development, climate and morphologic dating of fault scarps in Laguna Salada, Baja California, Mexico: Geomorphology, v. 102, p. 578-594, doi:10.1016j/geomorph.2008.06.001.

Spinler, J.C., Bennet, R.A., Anderson, M.L., McGill, S.F., Hreinsdottir, S., and McCallister, A., 2010, Present day strain accumulation and slip rates associated with southern San Andreas and eastern California shear zone faults from GPS: Journal of Geophysical Research, 115, B11407, doi:10.1029/2010JB007424.

Stone, J.O., 2000, Air pressure and cosmogenic isotope production, Journal of Geophysical Research: Solid Earth, vol. 105(B10), p. 23753-23759.

USGS and CGS (U.S. Geological Survey and California Geological Society), 2006, Quaternary fault and fold database for the United States, from USGS website: http://earthquakes.usgs.gove/hazards/qfaults/ (accessed October, 2015).

WGCP (Working Group California Earthquake Probabilities), 2008, The Uniform California Earthquake Rupture Forecast, Version 2 (UCERF 2): U.S. Geological Survey Open-File Report 2007-1437 and California Geological Survey Special Report 203, http://pubs.usgs.gove/of/2007/1437/ (accessed October 2015).

Yule, J.D. Sieh, K., 2003, Complexities of the San Andreas Fault near San Gorgonio Pass: Implications for large earthquakes: Journal of Geophysical Research, vol. 108, no. B11, 2548.

APPENDIX A: FIGURES

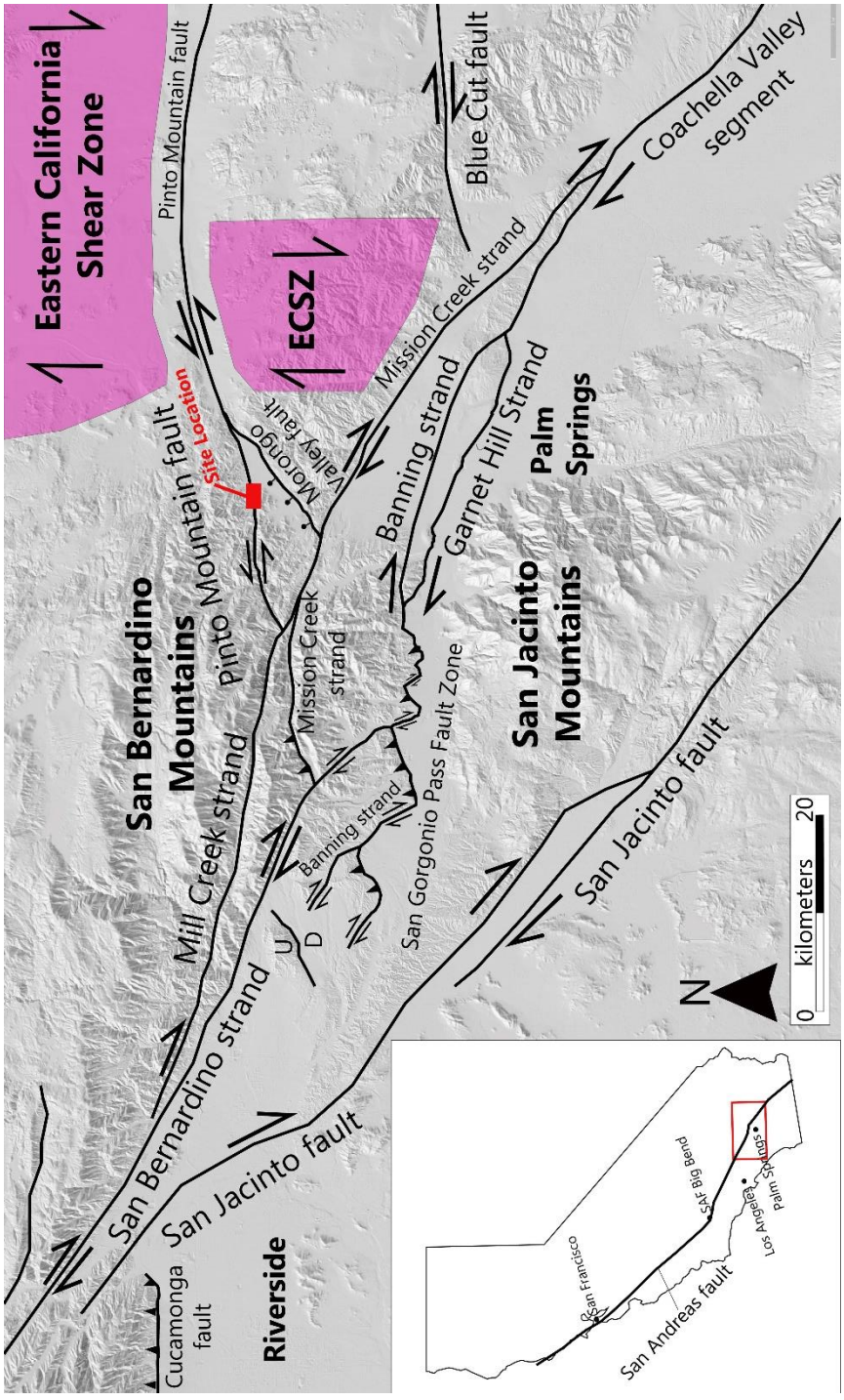

Figure 1: Simplified regional fault map of the southern San Andreas Fault (SAF) system through the San Gorgonio Pass (SGP). Inset map shows the SAF in California. Red box is location of this figure. Faults are modified from the USGS Quaternary fault and fold database. Arrows show sense of offset. Barbs indicate upthrown block along thrusts. Tick marks indicate downthrown block on inferred normal fault.

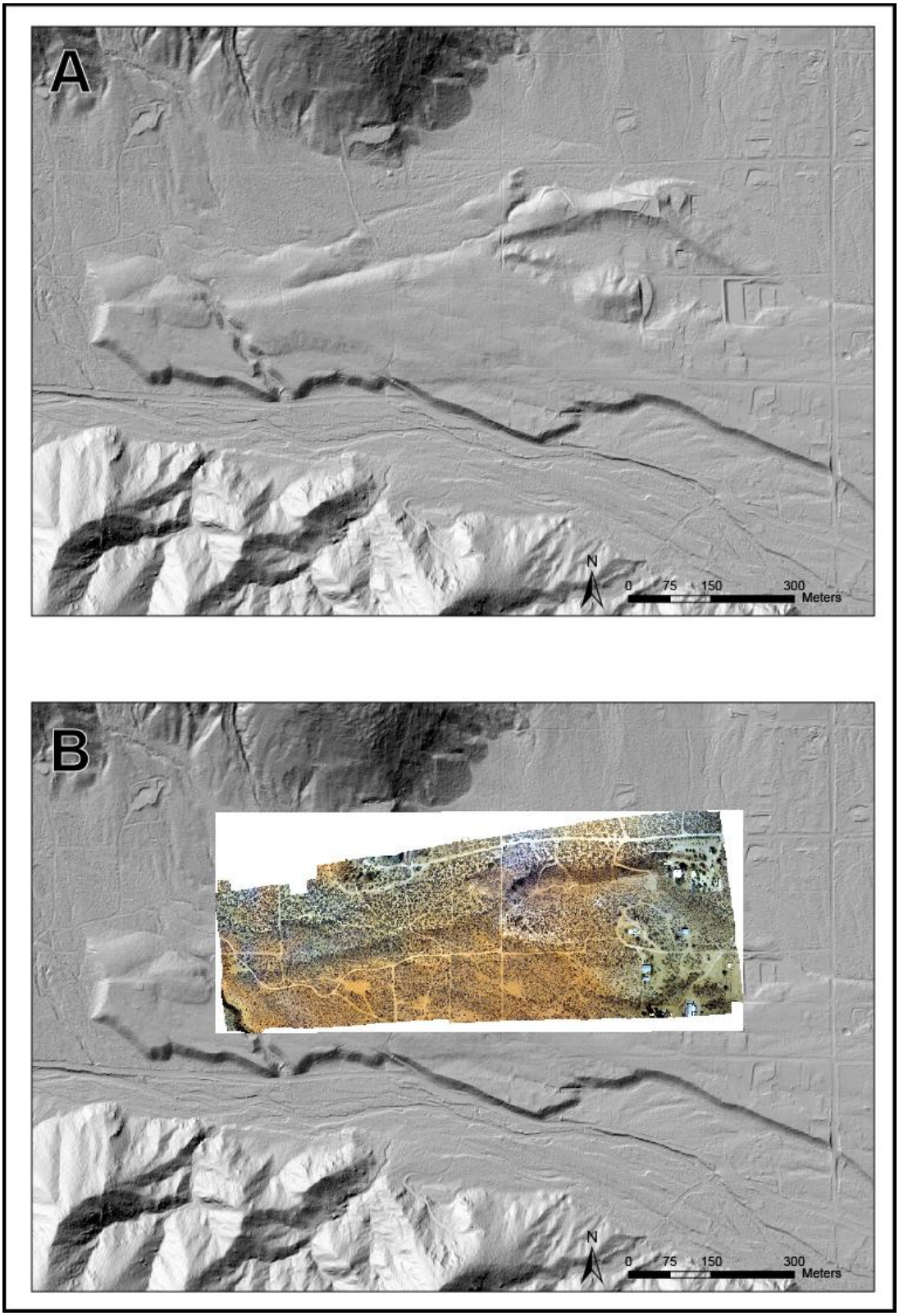

Figure 2: Lidar and structure from motion (SfM) data. A: Lidar data used as a basemap (NCALM, 2016). B: Lidar data overlain by Structure from Motion data. Colors are true photo colors not corrected during processing.

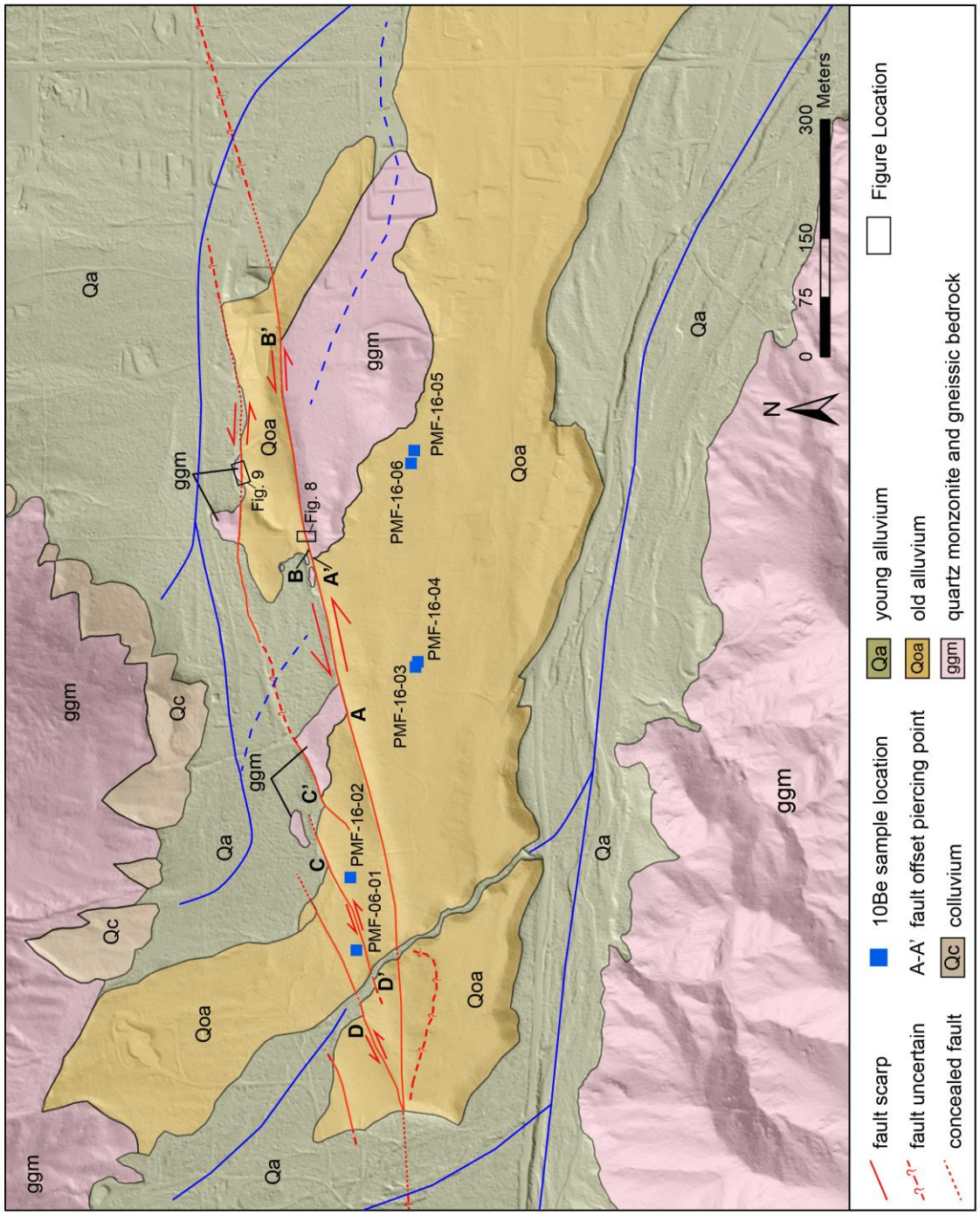

Figure 3: Geologic map of study area. Blue boxes are Cosmogenic ^{10}Be sample locations and are labeled with sample name. Offset piercing points are labelled with capital letters. Arrows indicate offset direction. Multiple strands of the PMF are shown cutting through old alluvium (Qoa), young alluvium (Qa) and offsetting bedrock (ggm). Blue lines show modern stream flow and dashed blue lines show paleo stream flow.

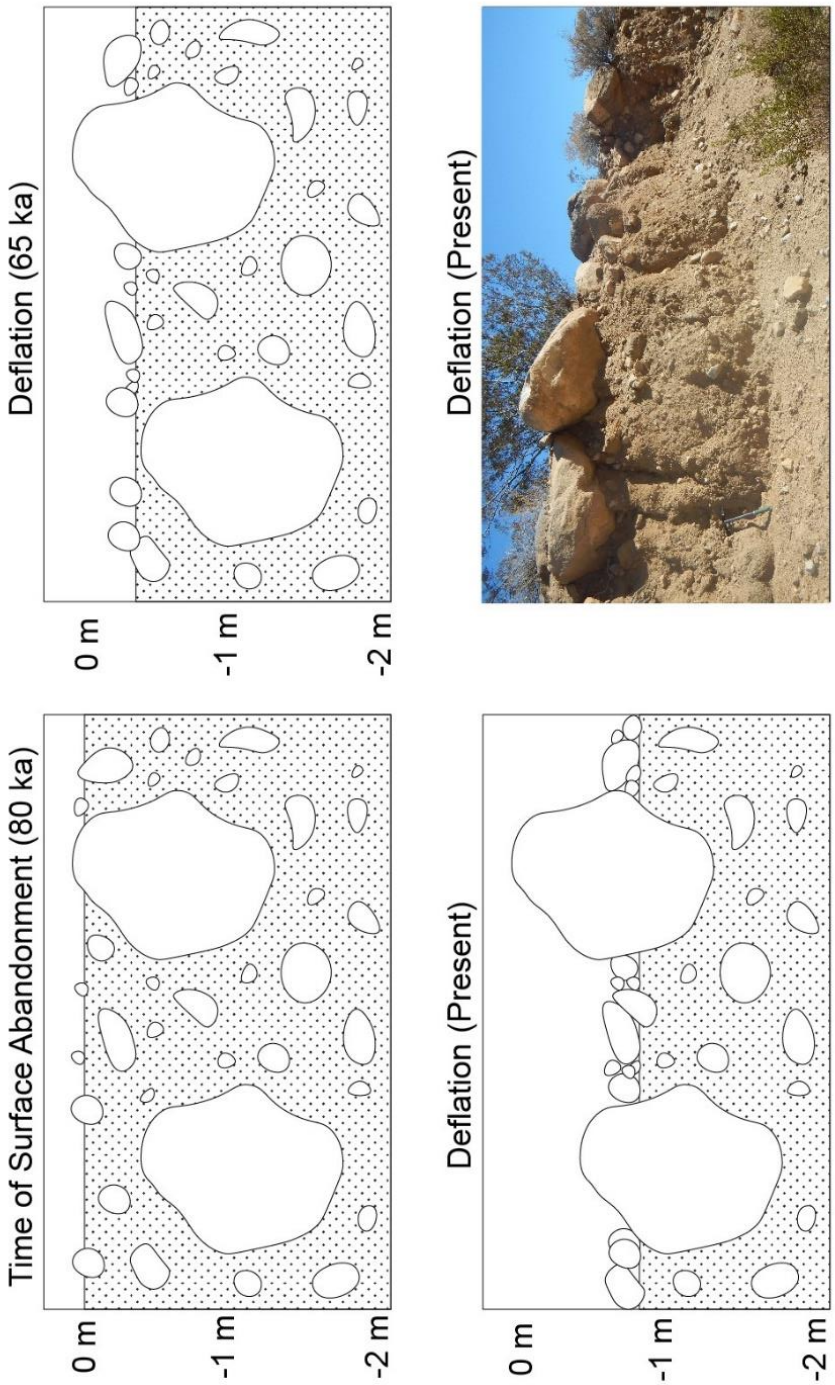

Figure 4: Process of surface deflation (or lowering). Cartoon shows fines eroding from the surface over time, resulting in settling/piling of gravels and cobbles. Photograph shows a cross section view of Qoa in a road cut in the southeast corner of the study area. Notice the similarities between the accumulation of cobbles and boulders right at the surface in the photograph and in the cartoon of Deflation (Present). Note: This amount of deflation is not typical for most of unit Qoa. This road cut is close to the edge of map unit Qoa where a relatively large amount of deflation has occurred.

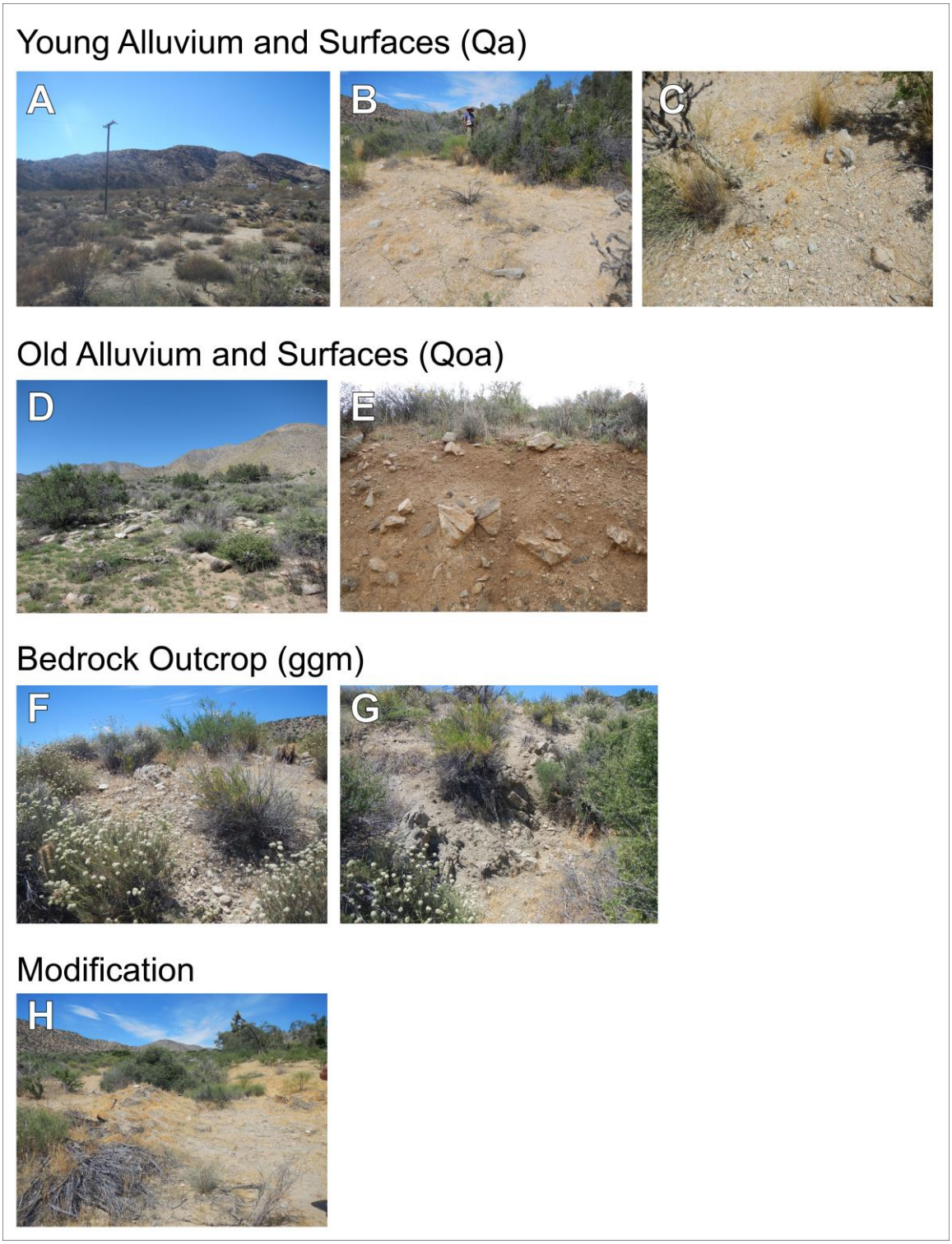

Figure 5: Photos of geologic units Qa and Qoa, and ggm outcrop. A-C: Qa; tan, sand to cobbles with few boulders. D: the surface of Qoa. E: a cross section view of Qoa in a road cut. F and G: examples of bedrock outcrops. H: modification to the Qa surface for road building and fire suppression.

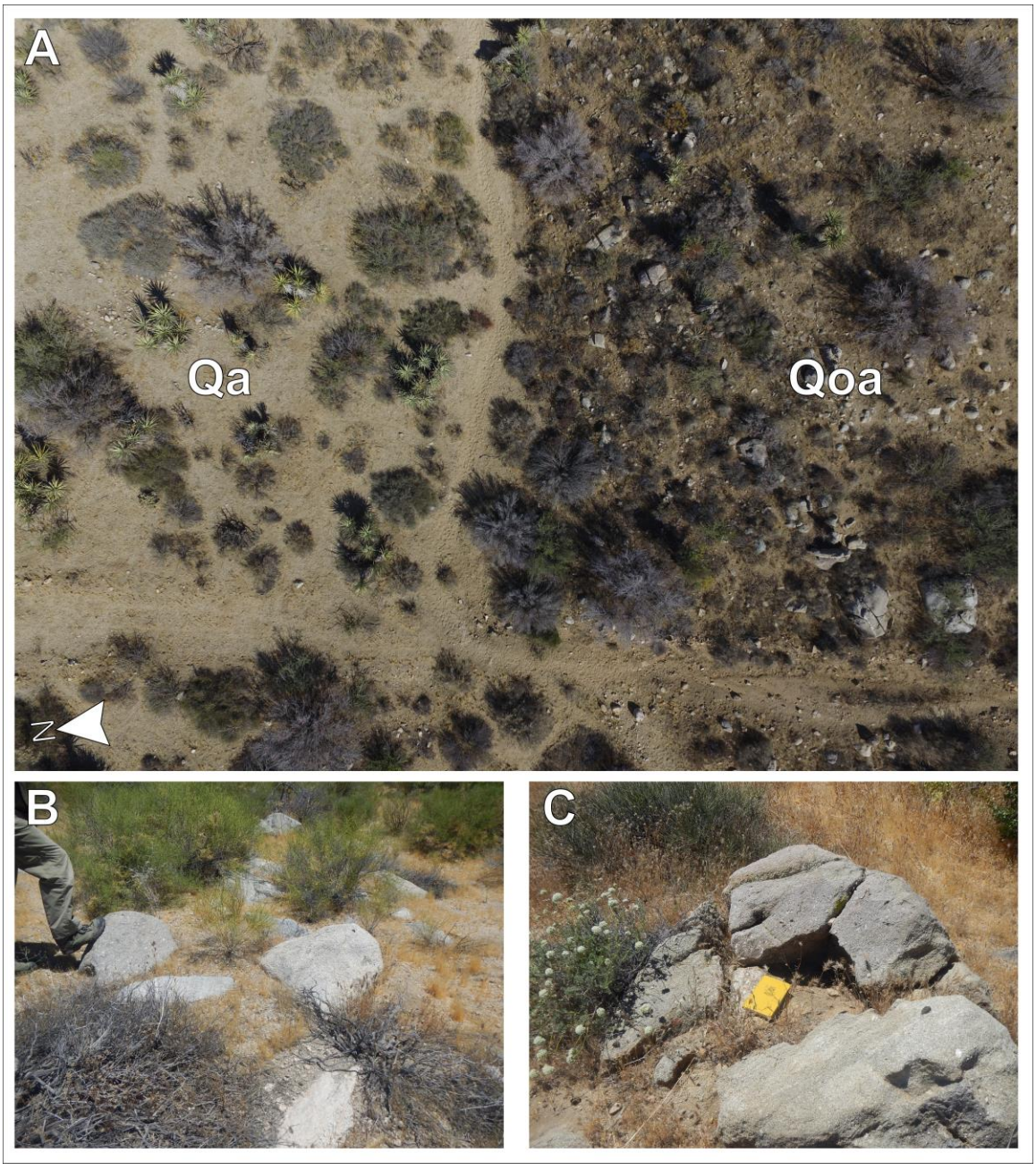

Figure 6: Boulders from Qa and Qoa. A: Comparison of overall general appearance of Qa (left) and Qoa (right) surfaces. B: Boulders on Qa surface, showing little to no varnish, and no spallation. C: Boulders on the Qoa surface, showing significant erosion, some varnish and spallation. Boulders with these characteristics were avoided during ^{10}Be sampling.

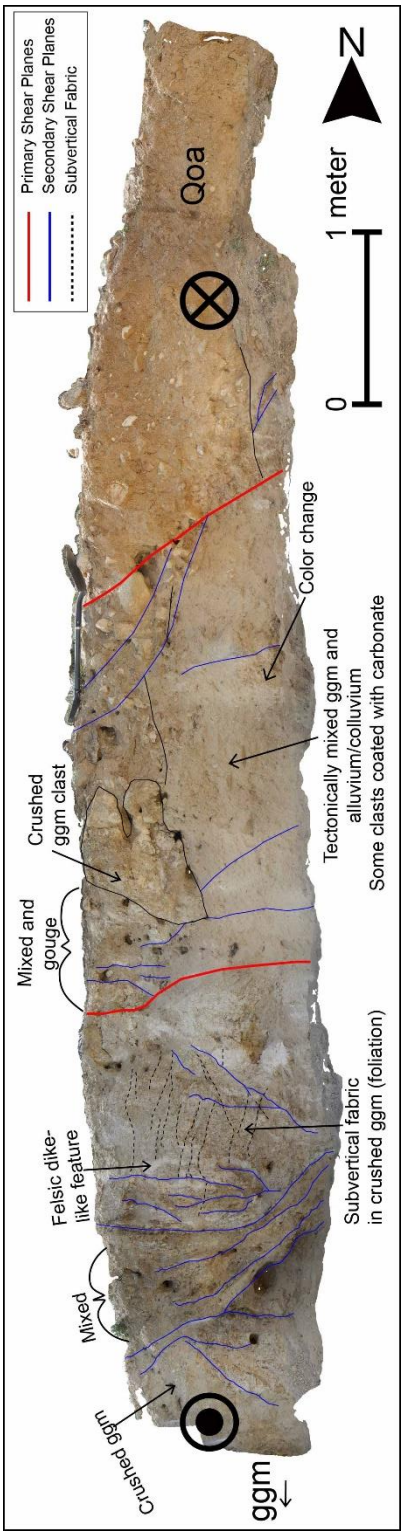

Figure 7: Outcrop of the main splay of the PMF, location shown on Figure 3. View looking west. Red lines indicate the primary shear planes, while blue lines indicate additional, less prominent shear planes (secondary). Black dashed lines are a sub-vertical fabric within the sheared ggm, possibly a secondarily sheared foliation. These features are currently filled with fine to medium sand.

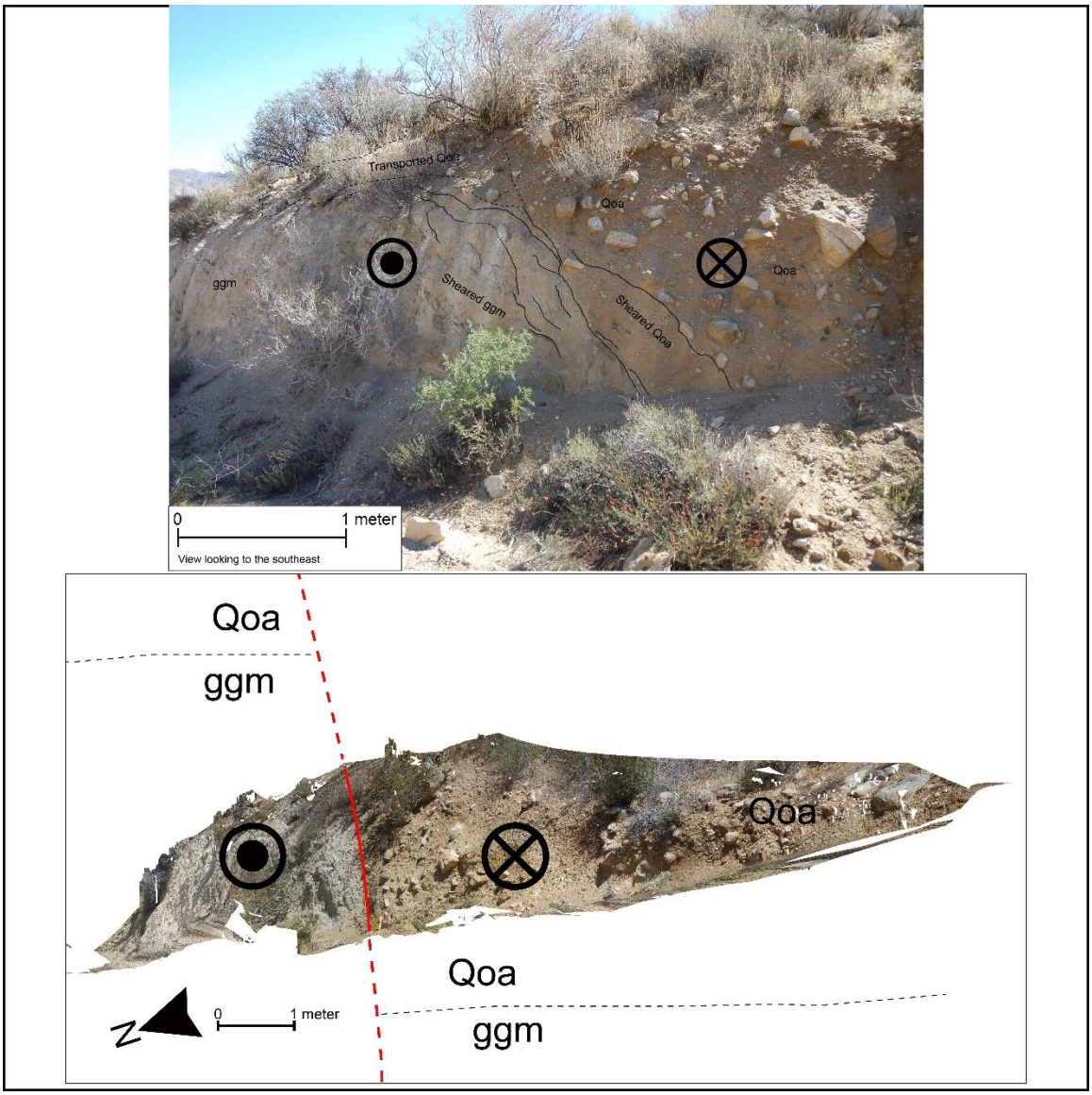

Figure 8: Outcrop of the north splay of the PMF. Location shown on Figure 3. Upper figure shows photograph along fault plane. Lower figure shows the 3D model developed with SfM in Agisoft Photoscan, looking along the fault plane. Both figures looking ~ESE.

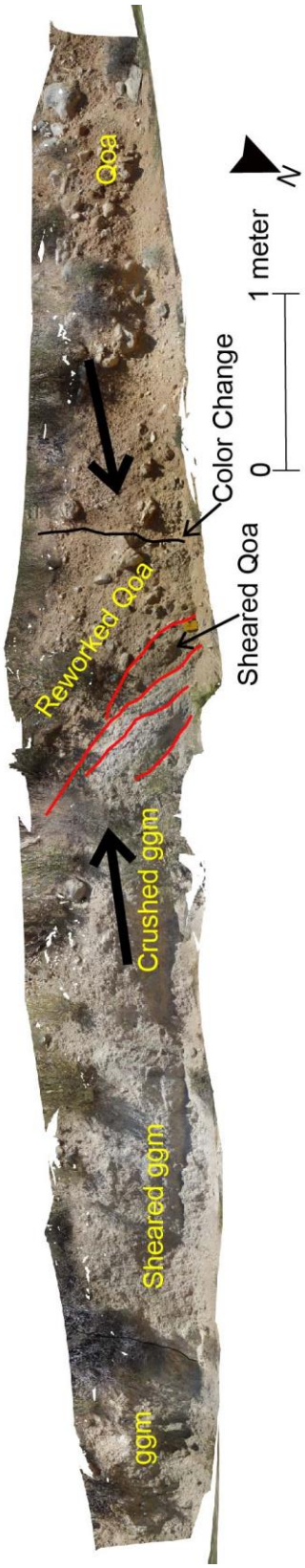

Figure 9: North strand outcrop view looking ~S at center. Figure is distorted. Showing fault outcrop that wraps around roughly slope roughly 40°-60°.

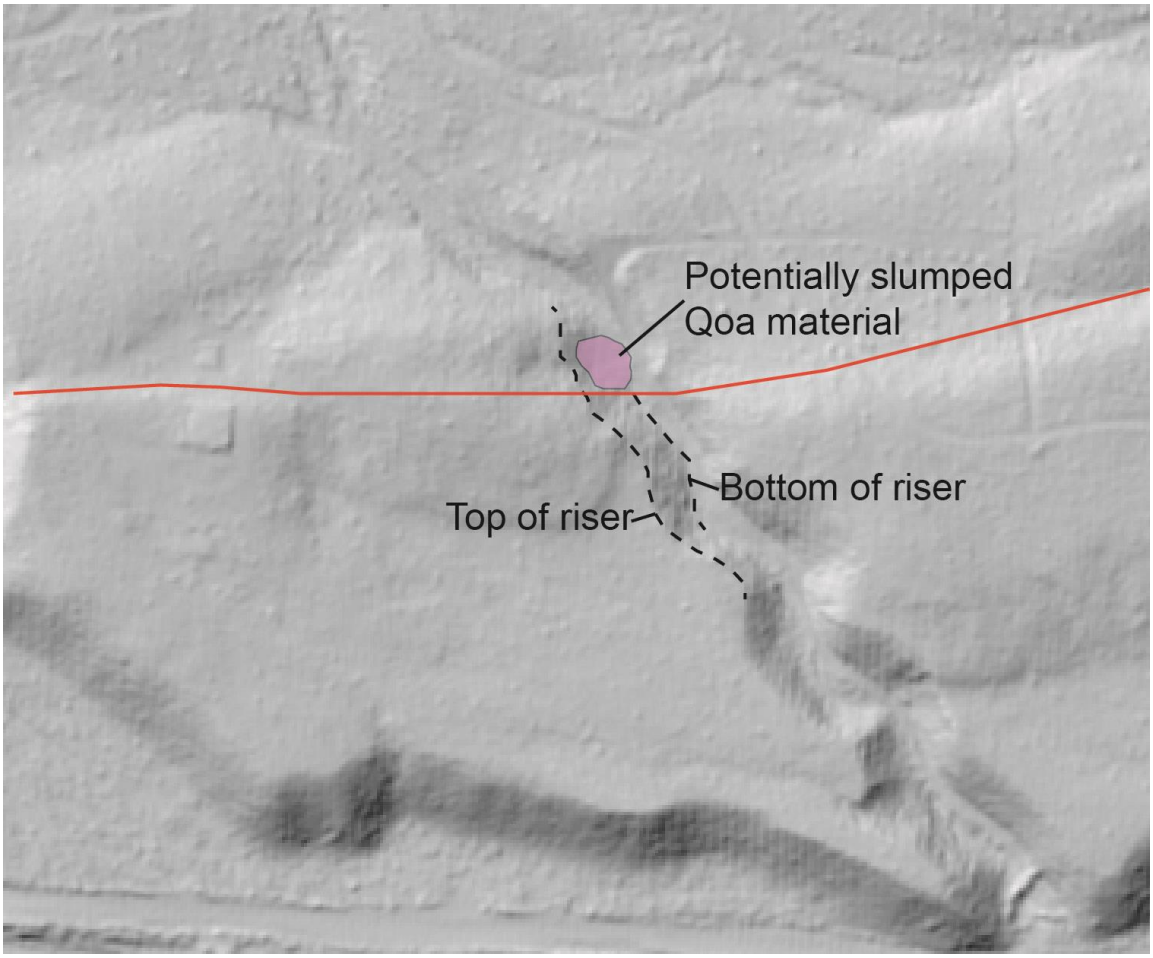

Figure 10: Lidar of the modern incised channel. Dashed lines show the trace of the top of the Qoa riser and the base of the riser (labeled). Light red line is the main splay of the PMF. Pink shading represents slumped Qoa material obscuring the base of the Qoa riser on the north side of the fault. I was unable to measure bottom-of-riser to bottom-of-riser offset because of the apparent slumping of Qoa material on the north side of the fault, but the top of the riser does not appear to be offset by the fault.

Figure 11: North splay scarp. View to east along scarp of north splay of PMF in Qa sediments. Up to the south separation likely produced by pure left-lateral slip bringing lower topography on north against higher topography on south.

Figure 12: 3D structure from motion model showing surface of study area. Looking SE. Red lines are fault splays. White areas showing zones of modification by heavy equipment, construction and/or road development.

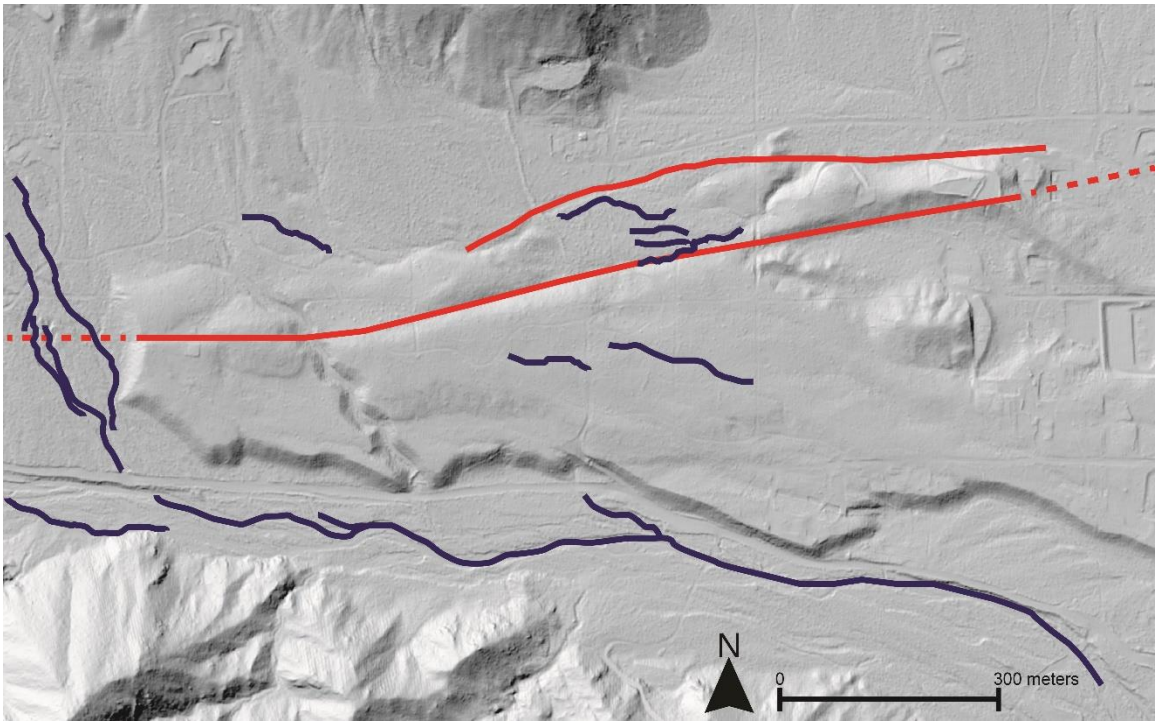

Figure 13: Lidar image showing stream sinuosity. Red lines are fault splays and northern escarpment in Qa, blue lines are traces of fluvial gullies. Note the smoothness of the north fault escarpment compared to the high sinuosity of the fluvial gullies.

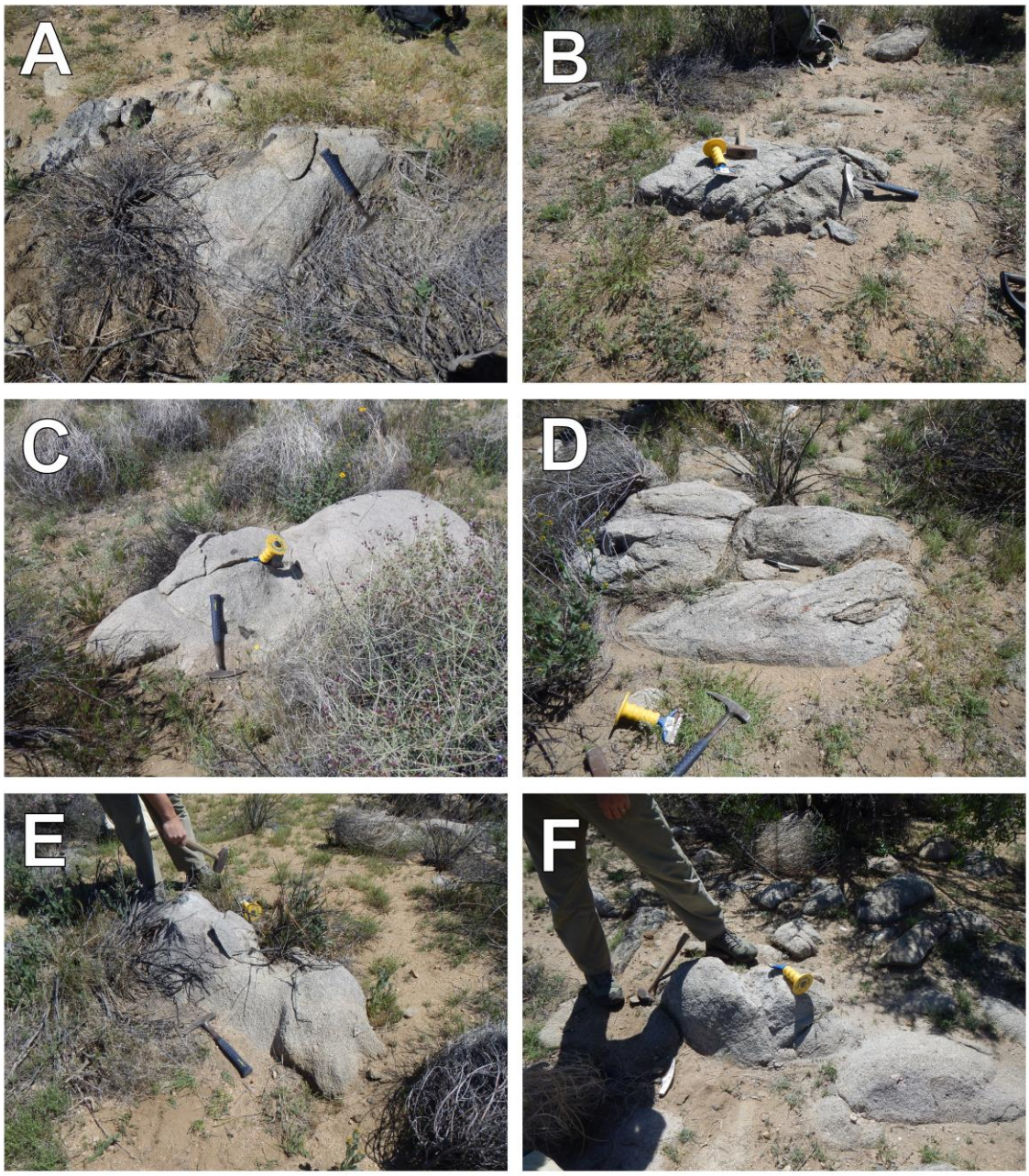

Figure 14: Photos of boulders sampled for Cosmogenic ^{10}Be surface exposure ages. A: PMF-16-01. B: PMF-16-02. C: PMF-16-03. D: PMF-16-04 E: PMF-16-05. F: PMF-16-06. Photos taken just prior to sampling, except for F, which was taken after sampling.

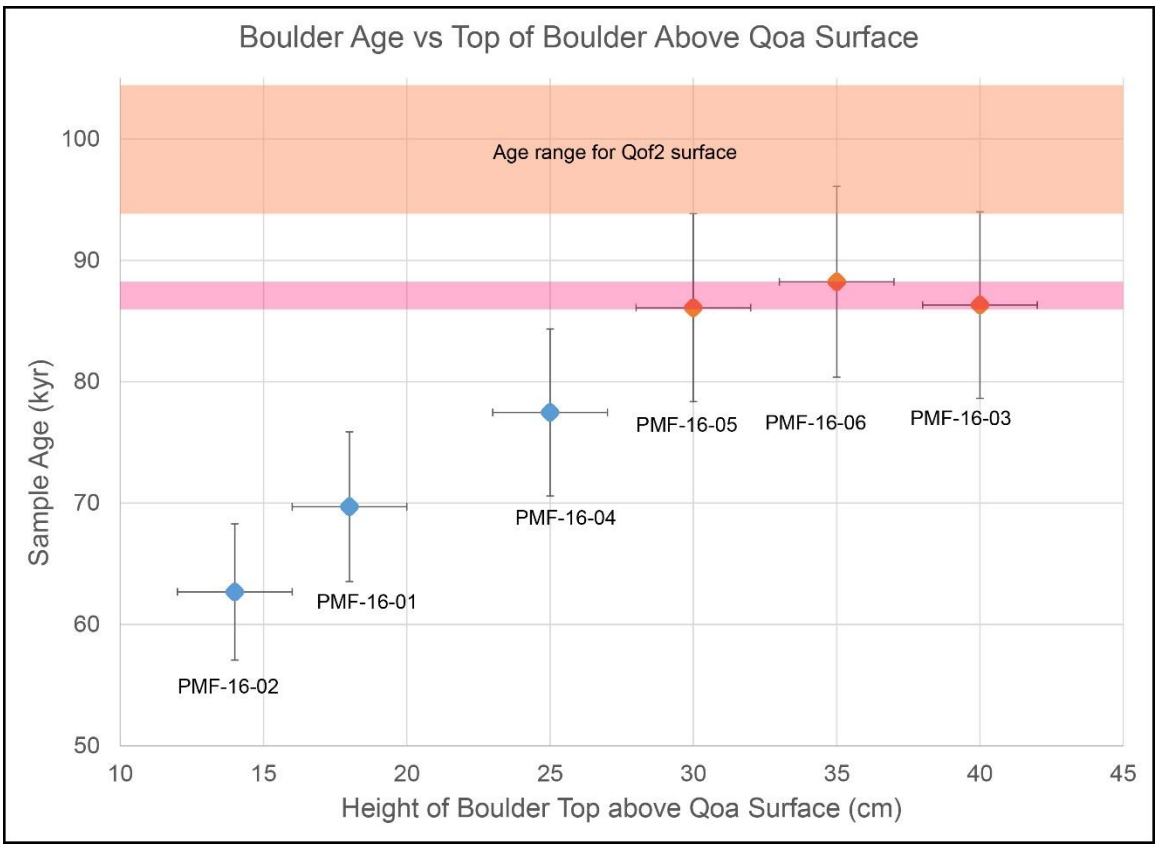

Figure 15: Sample age plot. Plot of sample age on x-axis vs height of the sampled boulder top above surface Qoa. Blue samples represent those that are exhumed as a result of deflation, orang samples were exposed at time of surface abandonment. Pink line represents surface age at time of deposition. Orange line represents age range for the Qof2 fan in the Mission Creek fan complex (Kendrick et al., 2015), that likely formed as part of the same regional fan building event that formed my fan Qoa. The three orange samples were used to calculate the weighted mean of the Qoa surface.

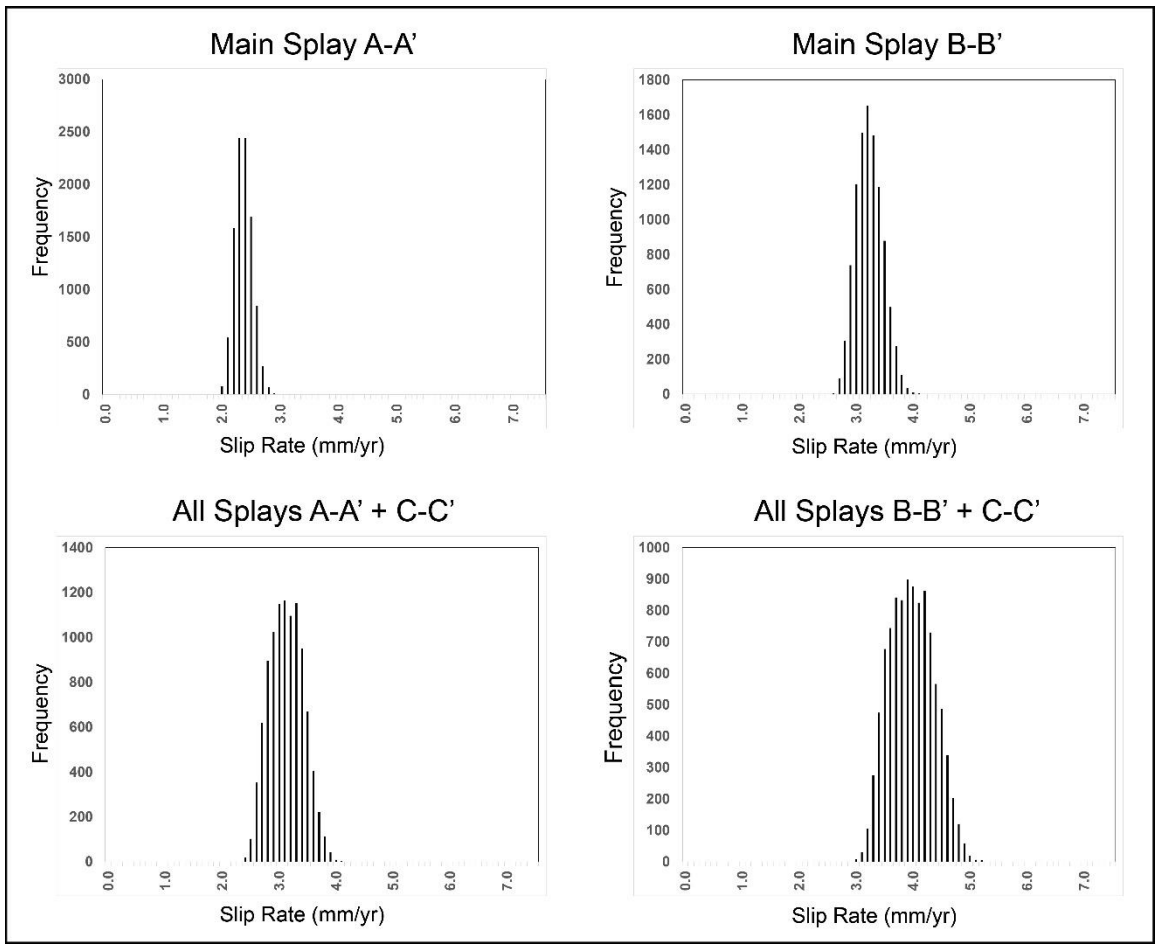

Figure 16: Histogram results of 10,000 Monte Carlo analyses of slip rate across the western PMF main splay (top) and all splays (bottom). Parameters used in this simulation are shown in Table 1. I determined slip rate as the mean value with errors of cumulative 95% minimum and 95% maximum values.

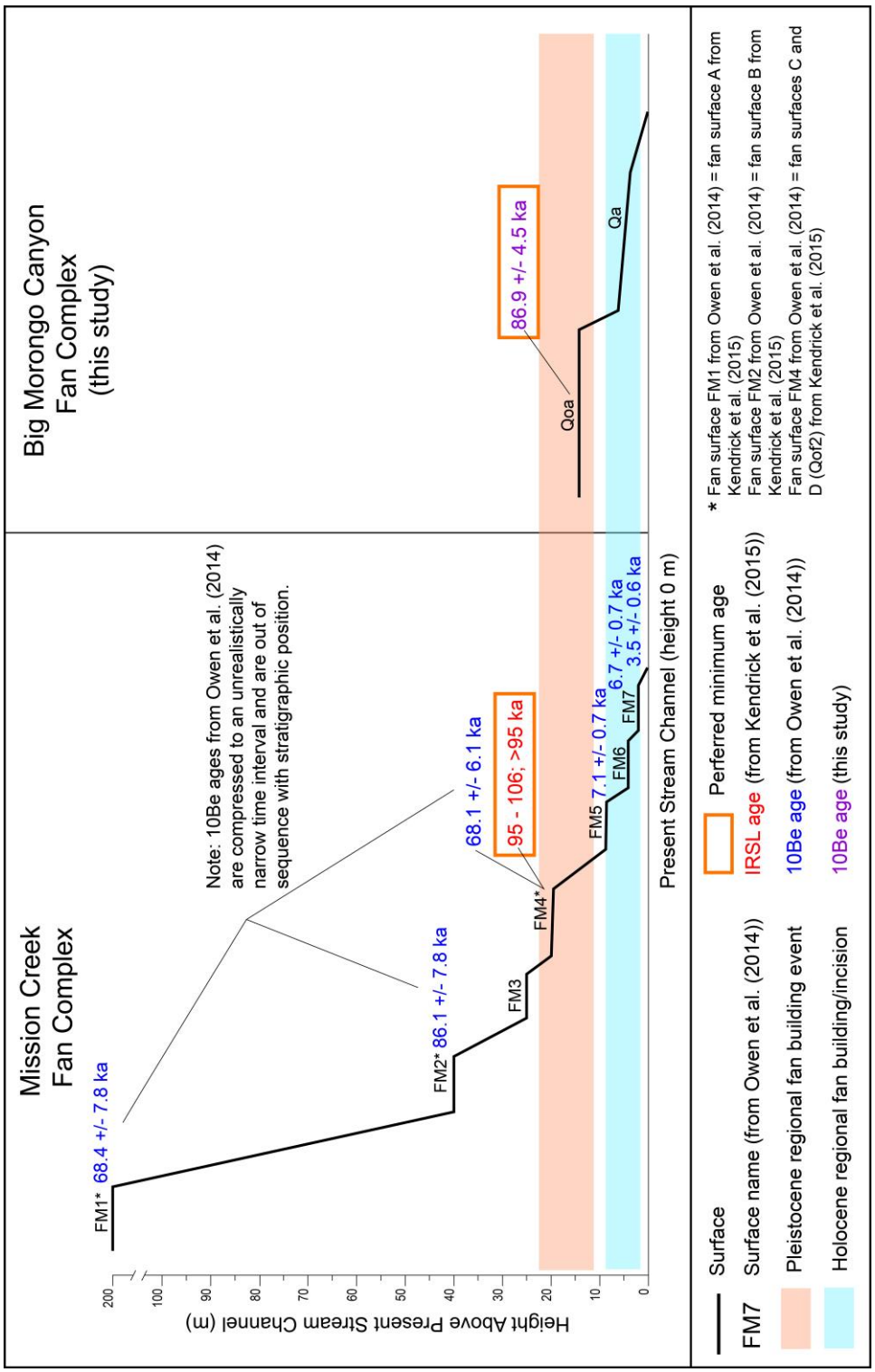

Figure 17: Schematic topographic profile of terrace levels of the Mission Creek fan complex and the Big Morongo Canyon fans. For Mission Creek, surface naming follows Owen et al. (2014) [Fm1-7]. Pink line represents possible Pleistocene regional fan correlation, blue shading represents possible Holocene regional fan correlation.

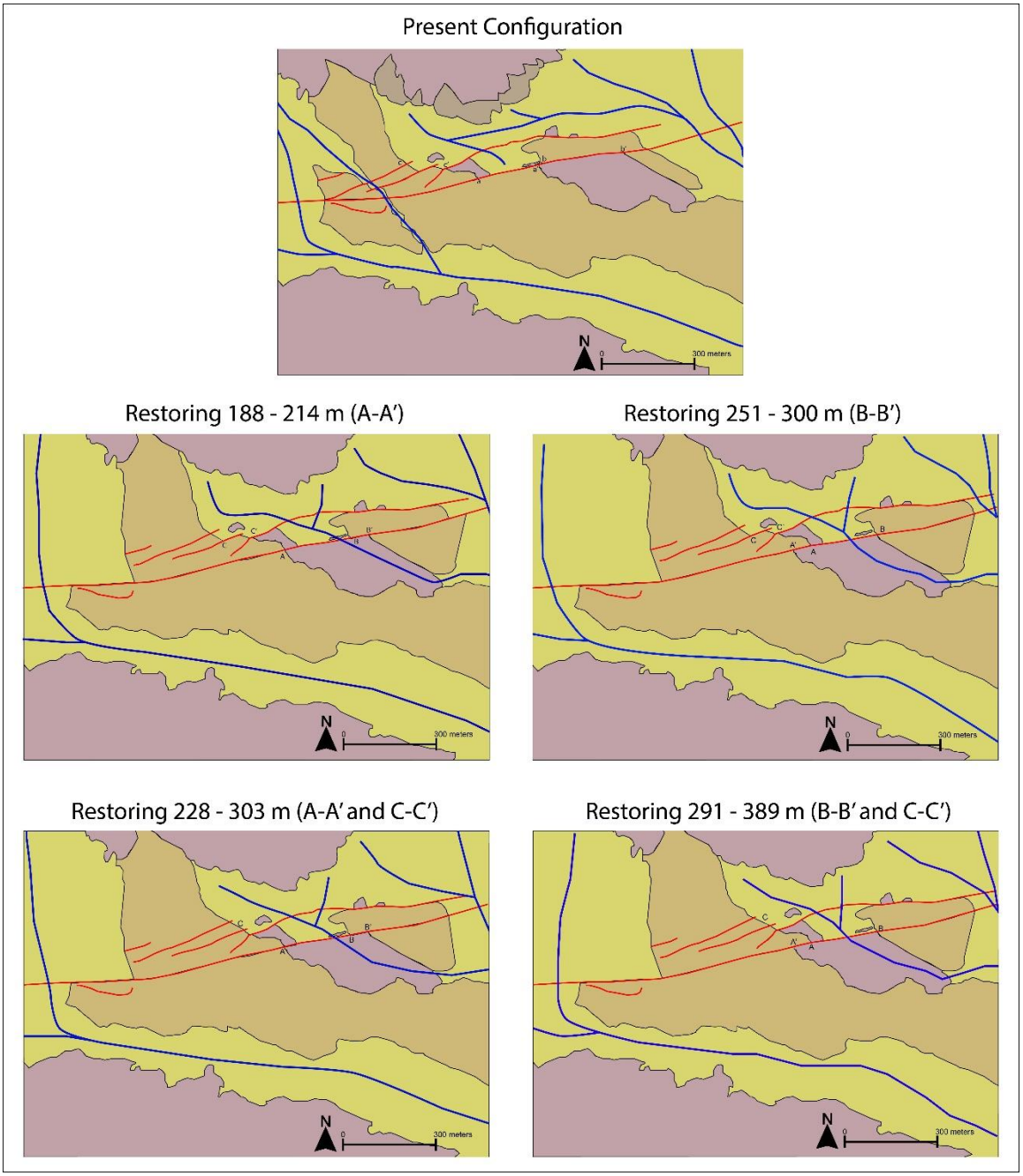

Figure 18: Restoration of offset across the PMF system. Unit colors consistent with those used in Figure 3. Red lines are fault splays. Blue lines show water flow paths. Direction of flow overall North to south and west to east. Left side of figure represents model in which additional occurred on the eastern margin of the paleochannel. Right side of figure represents model in which additional erosion occurred on the west side of the paleochannel.

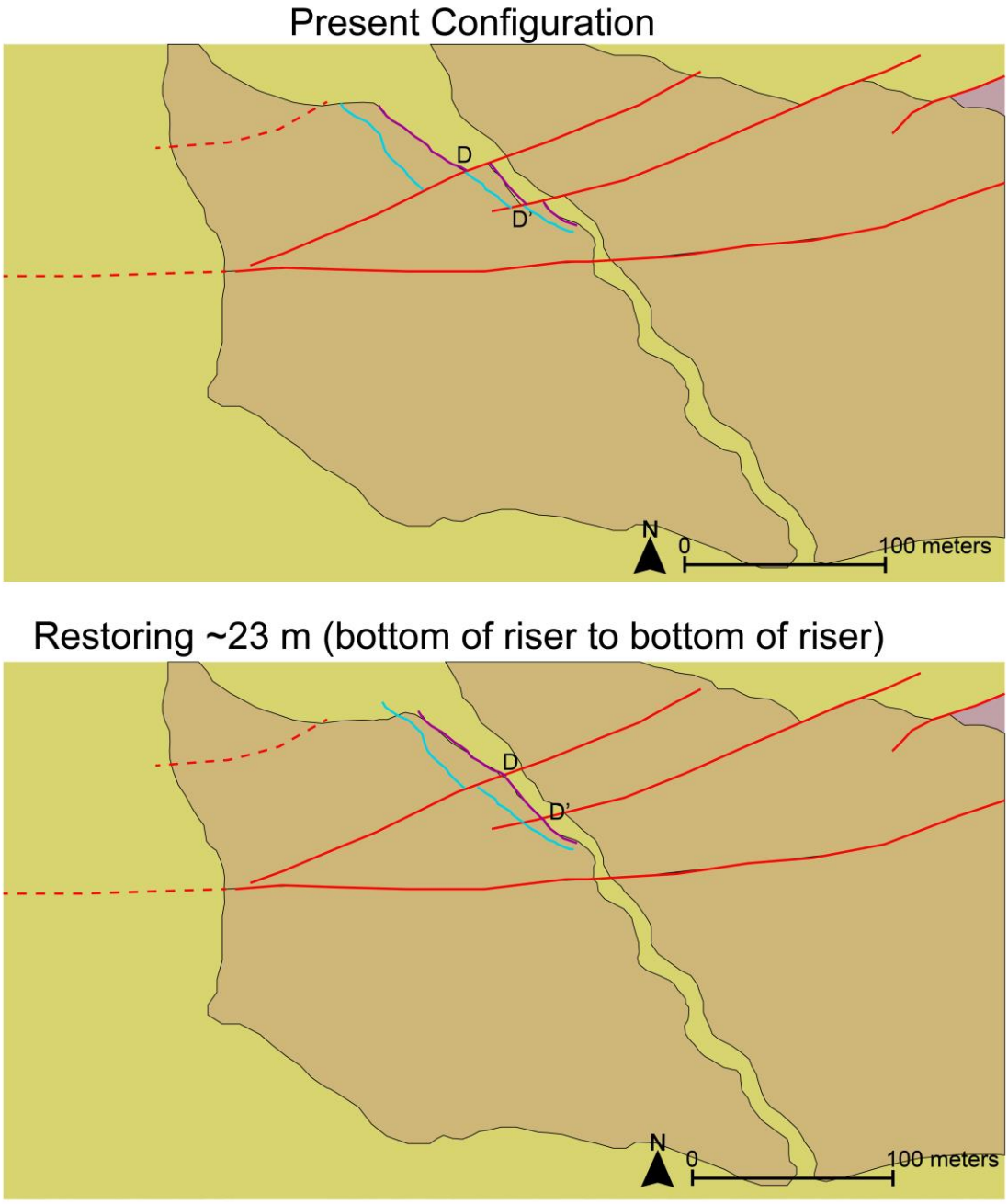

Figure 19: Reconstruction of offset D-D', the channel incised into Qoa surface. Note that no significant offset is observed at the main splay of the PMF (southern-most strand) because of high channel sinuosity. Bottom image restores ~22 m, which represents a base-of-riser to base-of-riser restoration.

APPENDIX B: TABLES

Table 1. Fault Offset and Monte Carlo Simulation Data. Slip rates calculated for main splay offsets (A-A' and B-B') and northern splay offset (C-C'). C-C' is considered additional offset to that observed on the main splay.

Geologic Feature			Geochronology (kyr)				Horizontal Offset (m)		Calculated Slip Rates (mm/yr)				
Offset Name	*Fault Splay*	*Marker*	*Mean Age*[a]	*1 Std. Error*	*Min. Age*	*Max. Age*	*Min.*	*Max.*	*Mean*	*Median*	*Mode*	*Cumulative 95% min*	*Cumulative 95% max*
A-A'	South (main splay)	Qoa/ggm contact	86.9	4.5	86.1	88.2	188	214	2.3	2.3	2.4	2.0	2.7
B-B'	South (main splay)	Qoa/ggm contact (buried)	86.9	4.5	86.1	88.2	251	300	3.2	3.2	3.2	2.7	3.7
C-C'	North (2 splays)	Qoa/ggm contact (buried)	86.9	4.5	86.1	88.2	40	89	0.7	0.7	0.8	0.5	1.1
D-D'	North (2 splays)	Incised modern channel	unconstrained				23	38	unconstrained				

[a]Weighted mean with 1 standard error of three oldest samples, PMF-16-03, PMF-16-05 and PMF-16-06

Table 2. Table reporting results for in situ cosmogenic ^{10}Be boulders from the Qoa surface

Sample	Location (°N/°W)	Elevation (m above sea level)	Thickness[a] (cm)	Production Rate (atoms g^{-1} yr^{-1})		Shielding Factor	Erosion Rate (mm/yr)	Quartz[d] (g)	Be Carrier (g)	10Be/9Be[e,f] ($x10^{-12}$)	10Be Concentration[g] (10^5 atoms g^{-1} of SiO_2).	Age[h,i] (ka)
				Spallation[b]	Muons[c]							
PMF-16-01	34.0814/ 116.5758	981	7	7.29	0.103	0.9969	0	35.603	0.2327	1.175 +/- 0.015	5.06 +/- 0.08	69.70 +/- 6.2
PMF-16-02	34.0815/ 116.5747	977	8	7.21	0.103	0.9969	0	35.618	0.2323	1.051 +/- 0.020	4.51 +/- 0.10	62.68 +/- 5.6
PMF-16-03	34.0807/ 116.5718	962	5	7.31	0.103	0.9974	0	35.646	0.2323	0.454 +/- 0.020	6.26 +/- 0.11	86.31 +/- 7.6
PMF-16-04	34.0807/ 116.5717	961	6	7.24	0.103	0.9974	0	35.83	0.2393	1.266 +/- 0.017	5.58 +/- 0.10	77.46 +/- 6.9
PMF-16-05	34.0807/ 116.5688	944	8	7.03	0.102	0.9974	0	35.51	0.2334	1.385 +/- 0.025	6.01 +/- 0.13	76.09 +/- 7.7
PMF-16-06	34.0807/ 116.5690	945	8	7.04	0.102	0.9974	0	35.68	0.2423	1.374 +/- 0.019	6.16 +/- 0.11	88.23 +/- 7.9

[a] Tops of all samples were exposed at surface.

[b] Constant (time-invariant) local production rate based on Lal (1991) and Stone (2000). Value calculated by CRONUS.

[c] Constant (time invariant) local production rate based on Heisinger et al., (200a,2002b). Value calculated by CRONUS.

[d] A density of 2.7 g cm^{-3} was used based on the monzo-granitic composition of boulders.

[e] Assuming 10Be half-life = 1.36 Ma

[f] Uncertainties are reported at a 1σ confidence level

[g] Blank of $1.58x10^{-14}$ +/- 0.017 ^{10}Be atoms was used to correct for background.

[h] Propagated uncertainties include error in blank, carrier mass and counting statistics. Propagated model errors include uncertainty in production rate pf ^{10}Be, and ^{10}Be decay constant.

[i] Boulder ages calculated using CRONUS version 2.3 (Balco et al., 2008).